Monocytes generated by interleukin-6-treated human hematopoietic stem and progenitor cells secrete calprotectin that inhibits erythropoiesis

Valentine Marchand, Lucie Laplane, Louis Valensi, Isabelle Plo, Marine Aglave, Aymeric Silvin, Florence Pasquier, Françoise Porteu, William Vainchenker, Dorothée Selimoglu-Buet, et al.

iScience

Article

Monocytes generated by interleukin-6-treated human hematopoietic stem and progenitor cells secrete calprotectin that inhibits erythropoiesis

Graphical abstract

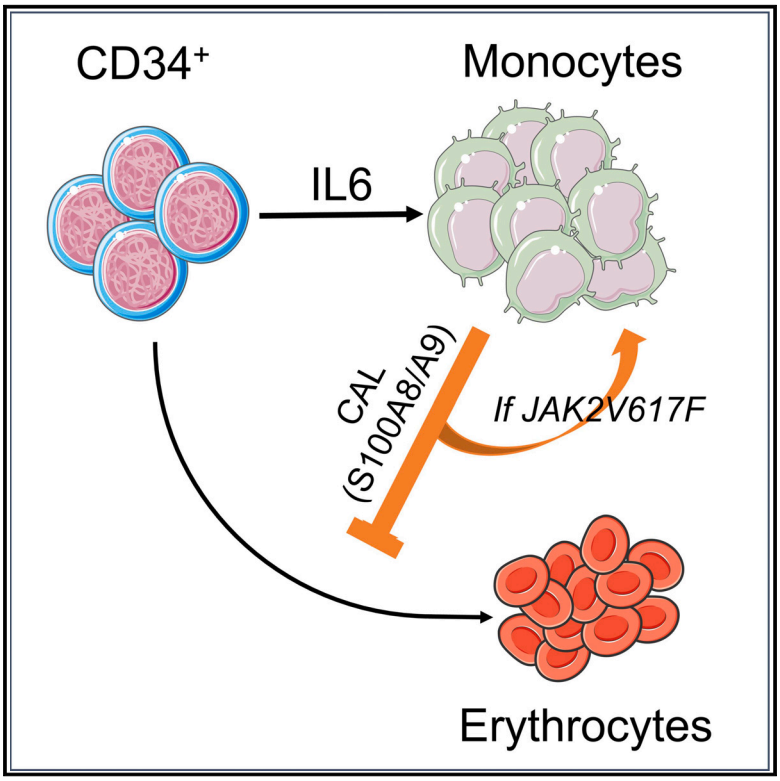

Authors

Valentine Marchand, Lucie Laplane, Louis Valensi, ..., Jean-Jacques Diaz, Michaela Fontenay, Eric Solary

Correspondence

eric.solary@gustaveroussy.fr

In brief

Pathology; Cell biology

Highlights

- IL-6 promotes the generation of monocytes secreting calprotectin
- Calprotectin inhibits erythroid progenitor differentiation
- JAK2-V617F amplifies hematopoietic effects of calprotectin
- A calprotectin signature is detected in bone marrow cells of various diseases

Marchand et al., 2025, iScience *28*, 111522
January 17, 2025
https://doi.org/10.1016/j.isci.2024.111522

CellPress

iScience

CellPress
OPEN ACCESS

Article

Monocytes generated by interleukin-6-treated human hematopoietic stem and progenitor cells secrete calprotectin that inhibits erythropoiesis

Valentine Marchand,[1] Lucie Laplane,[1,2] Louis Valensi,[1] Isabelle Plo,[1] Marine Aglave,[3] Aymeric Silvin,[4] Florence Pasquier,[5] Françoise Porteu,[1] William Vainchenker,[1] Dorothée Selimoglu-Buet,[1] Nathalie Droin,[1,3] Hana Raslova,[1] Virginie Marcel,[6] Jean-Jacques Diaz,[6] Michaela Fontenay,[7,8] and Eric Solary[1,9,10,*]

[1]INSERM U1287, Université Paris-Saclay, Gustave Roussy Cancer Center, Villejuif, France
[2]CNRS 8590, Université Paris 1 Panthéon-Sorbonne, Paris, France
[3]AMMICa, INSERM US 23, CNRS UMS 3655, Gustave Roussy Cancer Center, Villejuif, France
[4]INSERM U1108, Gustave Roussy Cancer Center, Villejuif, France
[5]Department of Hematology, Gustave Roussy Cancer Center, Villejuif, France
[6]Inserm U1052, CNRS UMR5286 Centre de Recherche en Cancérologie de Lyon, Lyon, France
[7]Université Paris Cité, Institut Cochin, CNRS UMR 8104, INSERM U1016, Paris, France
[8]Laboratory of Excellence for Red Blood Cells, GR-Ex, Paris, France
[9]Université Paris-Saclay, Faculté de Médecine, Le Kremlin-Bicêtre, France
[10]Lead contact
*Correspondence: eric.solary@gustaveroussy.fr
https://doi.org/10.1016/j.isci.2024.111522

SUMMARY

Elevated circulating levels of calprotectin (CAL), the S100A8/A9 heterodimer, are biomarkers of severe systemic inflammation. Here, we investigate the effects of CAL on early human hematopoiesis. CAL demonstrates limited impact on gene expression in stem and progenitor cells, in contrast with interleukin-6 (IL6), which promotes the expression of the *S100A8* and *S100A9* genes in hematopoietic progenitors and the generation of monocytes that release CAL. The main target of CAL is an erythroid-megakaryocyte progenitor (EMP) subset. CAL prevents both erythropoietin-driven differentiation of healthy progenitors and JAK2-V617F-driven erythropoiesis. In the context of JAK2-V617F, CAL also promotes the expression of *S100A8* and *S100A9* genes in monocytes. The signature of CAL effects is detected in the bone marrow progenitors of patients with myeloid malignancy or severe infection. These results position CAL as a mediator of IL6 effects on triggering anemia during inflammation, an effect that is amplified in the context of JAK2-V617F-driven hematopoiesis.

INTRODUCTION

Inflammation is an adaptive response to the homeostatic disturbance that involves soluble mediators and effector leukocytes. In response to damage and stress, cells release a variety of cellular constituents that trigger the production of inflammatory mediators with multiple effects on target tissue and beyond.[1] These inflammatory mediators include danger-associated molecular patterns (DAMPs), which act as extracellular danger signals. The alarmins S100A8 and S100A9, are the most abundant DAMPs in a variety of clinical disorders.[2] In the intracellular milieu, these calcium-binding proteins exist mostly as the heterodimeric complex S100A8/S100A9 termed calprotectin (CAL).[3] Animal models and clinical studies have shown the pivotal role of CAL in a wide range of sterile and infection-induced acute and chronic inflammatory diseases.[4] CAL is primarily released by activated phagocytes such as neutrophils and monocytes,[5] and interacts with and activates Toll-like receptor 4 (TLR4/MD-2)-expressing cells to promote inflammatory processes.[6]

Inflammation, regardless of its origin and location, stresses hematopoietic tissue in an attempt to maintain homeostasis. This stress involves soluble inflammatory mediators that act indirectly or directly on hematopoietic stem and progenitor cells (HSPCs) to promote the regeneration of the immune system.[7] In myocardial infarction, S100A8 and S100A9 released by activated and damaged phagocytes prime the NRP3 inflammasome in naive neutrophils that secrete interleukin-1 beta (IL1β), in turn promoting bone marrow granulopoiesis.[8] HSPCs also express TLRs and associated molecules and sense lipopolysaccharides.[9] Therefore, these cells may also respond to CAL. Elevated circulating levels of CAL, identified as a strong predictive biomarker of severe SARS-CoV-2 infection,[10] were correlated with dysregulated hematopoiesis.[11–13] However, the direct effects of CAL on early human hematopoiesis remain poorly explored.

The present study investigated the effects of CAL on early human hematopoiesis *ex vivo*. In the context of systemic inflammation, CAL is released together with multiple cytokines,

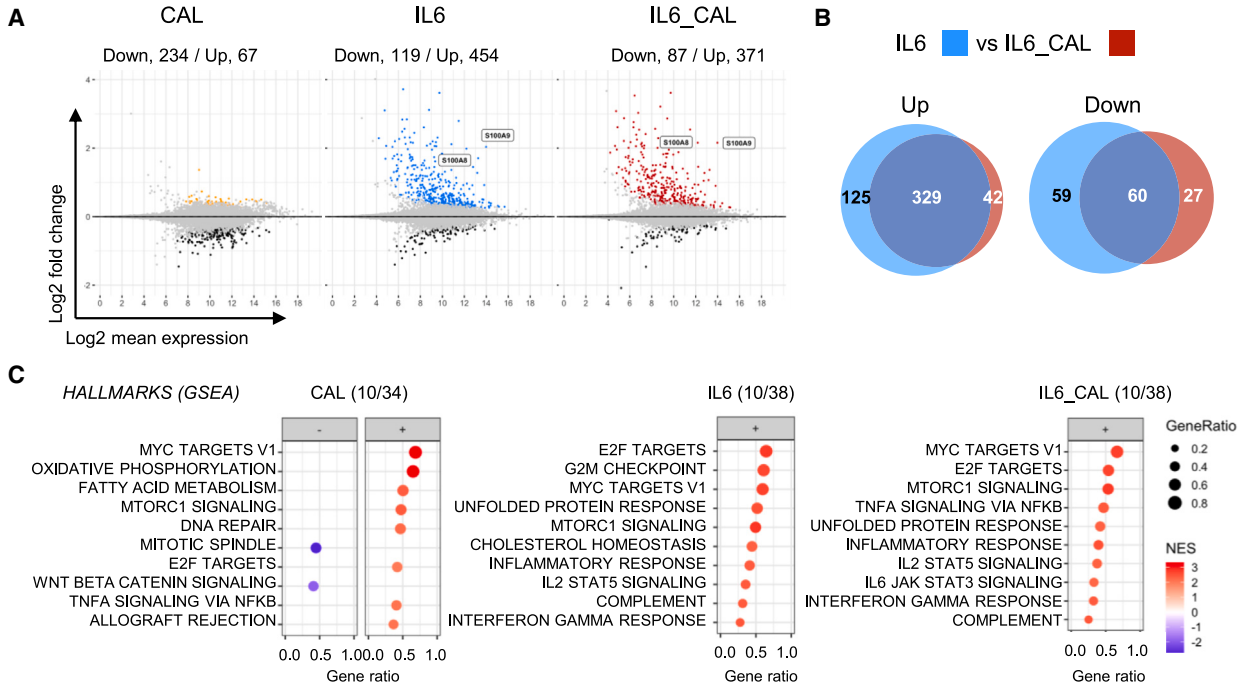

Figure 1. IL6 promotes *S100A8* and *S100A9* gene expression in hematopoietic progenitors

Healthy donor CD34$^+$ bone marrow cells were left untreated or treated for 24 h with calprotectin (CAL, 10 μg/mL), interleukin-6 (IL6, 100 ng/mL), or their combination (IL6_CAL) in the absence of growth factors before bulk RNA sequencing. $N = 3$. (A) MA plot of the decreased log fold change of the differentially expressed genes (DEGs) between treated and untreated samples. Down/Up indicates the number of significant DEGs.

(B) Venn diagram of upregulated and downregulated genes in IL6 (blue)- versus IL6_CAL (red)-treated cells compared to untreated cells.

(C) Pathway analysis of hallmark genes using gene set enrichment analysis (GSEA) under the indicated conditions (the top 10 pathways with the highest absolute NES are depicted out of the indicated number of significantly modified pathways in each condition). See also Figure S1.

including the prototypical acute phase response protein interleukin-6 (IL6).[14] We compared the effects of CAL on early human hematopoiesis to those of IL6, as IL6 increases myeloid cell output, both in mice[14] and in humans,[15] and to those of CAL + IL6 combination as both cytokines are usually released simultaneously.[11]

Given the propensity of patients with myeloid malignancies such as myelofibrosis (MF) to develop severe inflammatory reactions,[16,17] we also compared the response of HSPCs collected from healthy donors (HDs) and patients with MF to CAL. Our results point to CAL as an inhibitor of erythropoiesis, which is amplified by IL6 and, in the context of MF, by a feedforward loop involving monocytes.

RESULTS

Interleukin-6 promotes *S100A8* and *S100A9* gene expression in hematopoietic progenitors

We performed *ex vivo* culture of CD34$^+$ HSPCs collected from adult HD bone marrow in the absence or presence of IL6, CAL or their combination (IL6_CAL) at concentrations (IL6, 100 ng/mL; CAL, 10 μg/mL) detected in the peripheral blood plasma of patients with severe infection.[10,11,15] Frozen CD34$^+$ HSPCs were thawed and allowed to recover in the presence of Stem Cell Factor (SCF), FLT3-ligand (FLT3-L) and thrombopoietin (TPO) for 48 h. These cells were further cultured for 24 h before bulk RNA sequencing was performed. Treatment with IL6 alone or in combination with CAL promoted an increase in the expression of the *S100A8* and *S100A9* genes (Figures 1A and 1B).

According to gene set enrichment analysis (GSEA) of hallmark pathways, IL6 and IL6_CAL mostly promoted the cell cycle and metabolic and inflammatory pathways (Figure 1C). CAL alone had limited effects on gene expression in HSPCs (Figure 1A); nevertheless, it activated the oxidative phosphorylation pathway.

These initial results were validated in CD34$^+$ cells cultured for 48 h before performing bulk RNA sequencing (Figures S1A–S1C). Having defined common sets of genes robustly deregulated by IL6 or IL6_CAL at both 24 h and 48 h (Figure S1D), hallmark pathway overrepresentation analysis (ORA) revealed the activation of inflammatory signaling pathways (Figure S1E).

Deconvolution performed by gene set variation analysis (GSVA) (Table S1) revealed an IL6-induced increase in the monocyte signature, while the erythro–megakaryocyte signature decreased (Figure S1F). Together, IL6 increased *S100A8* and *S100A9* gene expression in HSPCs and could promote monocyte differentiation at the expense of erythroid differentiation.

Interleukin-6 promotes calprotectin secretion by immature monocytes

To further explore the effects of CAL and IL6 on early hematopoiesis, we incubated CD34$^+$ cells from four HDs for 7 days in the presence of SCF, FLT3-L and TPO without and with CAL, IL6

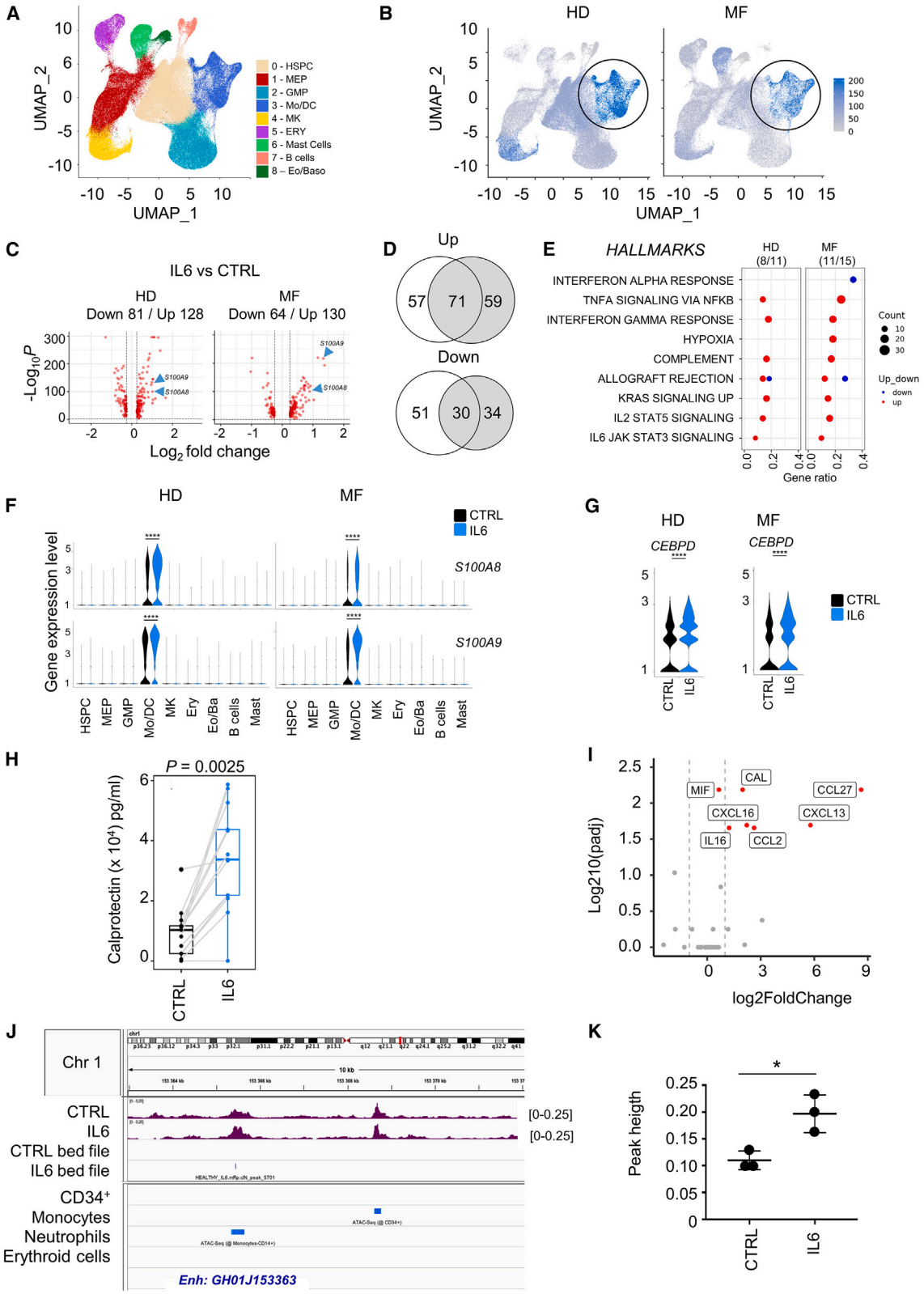

(legend on next page)

and IL6_CAL before collecting cells and culture supernatant. We performed the same experiment with CD34$^+$ cells collected from three patients with JAK2-V617F-mediated MF to determine if mutated CD34$^+$ cells would react differently to CAL (Figure S2A).

A total of 135,545 cells from 4 HDs and 111,725 cells from 3 patients with MF were analyzed by single-cell RNA sequencing (scRNA-seq) using the 10X Chromium droplet-based platform. We pooled the data from 28 samples (7 donors, 4 conditions per donor) and subjected them to dimensionality reduction using the Uniform Manifold Approximation and Projection (UMAP) algorithm for dimension reduction. Based on gene expression and cell type signature scores (Table S1), we identified 9 clusters, separating populations of HSPCs, megakaryocyte-erythroid progenitors (MEPs), granulomonocyte progenitors (GMPs), monocytes and dendritic cells (Mo/DCs), megakaryocytes (MKs), erythroid cells (ERYs), eosinophils and basophils (Eo/B), B cells and mast cells (Figures 2A and S2B; Table S2).

Within 7 days, IL6 increased the number of cells generated by HD CD34$^+$ cells, while the number of cells generated by MF CD34$^+$ cells remained unchanged (Figure S2C). IL6 ± CAL significantly increased the fraction of HSPCs and GMPs generated by HD CD34$^+$ cells at the expense of MEP fraction (Figure S2D). Nevertheless, the absolute number of MEPs remained stable (Figure S2E).

By coloring the cells on UMAPs according to the number of differentially expressed genes (DEGs) between the control and IL6 treatment conditions, we observed that, in both the HD and MF samples, the main impact of IL6 was on the Mo/DC population (Figure 2B**, circles**; Table S3). The number of DEGs generated upon IL6 exposure in this population was roughly the same in the HD (n = 209) and MF (n = 194) samples (Figures 2C and 2D). According to the ORA of hallmark pathways, IL6 increased the expression of genes involved in inflammatory pathways (Figure 2E).

The upregulated expression of the *S100A8* and *S100A9* genes observed in Mo/DCs generated in the presence of IL6 (Figures 2C and 2F) correlated with the increased expression of the *CEBPD* gene (Figure 2G), which encodes a well-identified player in alarmin gene expression.[18] Higher clustering resolution focused on Mo/DCs (Figure S2F) suggested that, in both HD and MF samples, the main impact of IL6 was on immature monocytes (Figures S2G and S2H).

We measured the expression of 41 cytokines in the culture supernatant collected on day 7 in a total of 11 HD cell cultures. IL6 significantly increased the secretion of CAL (Figure 2H) together with several pro-inflammatory cytokines that include chemo-attractants for immune cells (IL16, CCL27, and CXCL16 for T cells and CXCL13 for B cells) and MIF (Macrophage migration inhibitory factor) that modulates innate immunity and macrophage functions (Figure 2I).

ATAC-seq (assay for transposase-accessible chromatin with sequencing) of the bulk of cells generated from HD CD34$^+$ cells cultured for 7 days indicated that IL6 triggered chromatin opening at the level of a monocyte-specific enhancer that is common to the *S100A8* and *S100A9* genes (Figures 2J and 2K).

Then, we used cord blood CD34$^+$ cells exposed to SCF and M-CSF for 7 days in the absence or presence of IL6 before monitoring cell phenotype and *S100A8/A9* gene expression. We observed an increased production of monocytes with an accelerated acquisition of CD64 and CD300E cell surface markers and validated the increased expression of *S100A8* and *S100A9* genes in these cells (Figure S3). Together, IL6 promotes the generation of Mos/DCs that overexpress the *S100A8* and *S100A9* genes.

The effects of calprotectin on monocytes are restricted to myelofibrosis samples

In contrast to IL6 (Figure S2C), CAL alone did not significantly modify the total number of cells generated on day 7 by HD CD34$^+$ cells, while it decreased that generated by MF CD34$^+$ cells (Figure S4A). UMAP visualization of DEGs on day 7 indicated that the effects of CAL on Mo/DCs were specific to those generated by MF CD34$^+$ cells (Figure 3A**, circles**). The expression of 329 genes was rewired by CAL in Mo/DCs generated by MF cells, compared to only 15 DEGs in Mo/DCs generated by HD cells (Figure 3B). When IL6 was combined with CAL, the growth of HD CD34$^+$ cells increased, while the growth of MF CD34$^+$ cells still decreased (Figure S4A).

In HD cell culture, the number of genes whose expression was modified by IL6_CAL in the Mo/DC population (n = 255, Figures 3A and 3B) was close to that observed with IL6 alone (n = 209, Figures 2C and 3C). In MF culture, the number of genes whose expression was modified by IL6_CAL in the Mo/DC population (n = 580, Figures 3A and 3B) was much greater than that

Figure 2. IL-6 promotes calprotectin production by immature monocytes

(A) UMAP profile of cells generated by CD34$^+$ cells collected from HDs (n = 4) and patients with MF (n = 3) and cultured for 7 days in a liquid medium without or with CAL, IL6, or their combination.

(B) UMAP visualization of the number of DEGs in HD and MF samples after 7 days of treatment with IL6.

(C) Volcano plots of DEGs in cluster 3 (Mono/DC) generated from HD and MF samples treated with IL6.

(D) Venn diagrams comparing DEGs in cluster 3 (Mono/DC) generated from HD (in white) and MF (in gray) CD34$^+$ cells treated with IL6.

(E) Pathway analysis based on DEGs identified in cluster 3 (Mo/DC) in HD and MF samples.

(F) Violin plot of *S100A8*, *S100A9,* and *S100A12* gene expression in the 9 clusters generated by HD and MF CD34$^+$ cells without (in black) and with (in blue) IL6. Unpaired Wilcoxon rank-sum test; **** padj <0.0001 (see Table S3).

(G) Violin plots of *CEBPD* gene expression in HD and MF samples, untreated (CTRL) and IL6 treated. Unpaired Wilcoxon rank-sum test; **** padj <0.0001 (see Table S3).

(H) CAL levels are measured in individual samples cultured without and with IL6 for 7 days. Wilcoxon paired test.

(I) Cytokine levels in the culture supernatant of HD CD34$^+$ cells collected on day 7 (red: up with padj <0.05, hatched lines indicate a log2FoldChange of −1 and 1).

(J and K) Bulk ATAC sequencing of healthy donor CD34$^+$ cell-derived cells collected on day 7 of liquid culture without or with IL6 (n = 3). (J) The enhancer sequence identified in monocytes is shown as a blue rectangle. (K) Peak height measured for *S100A8* and *S100A9,* which are common monocyte-specific enhancers, in samples treated without and with IL6 (mean ± SD; paired T-test; *p < 0.05). See also Figures S2 and S3.

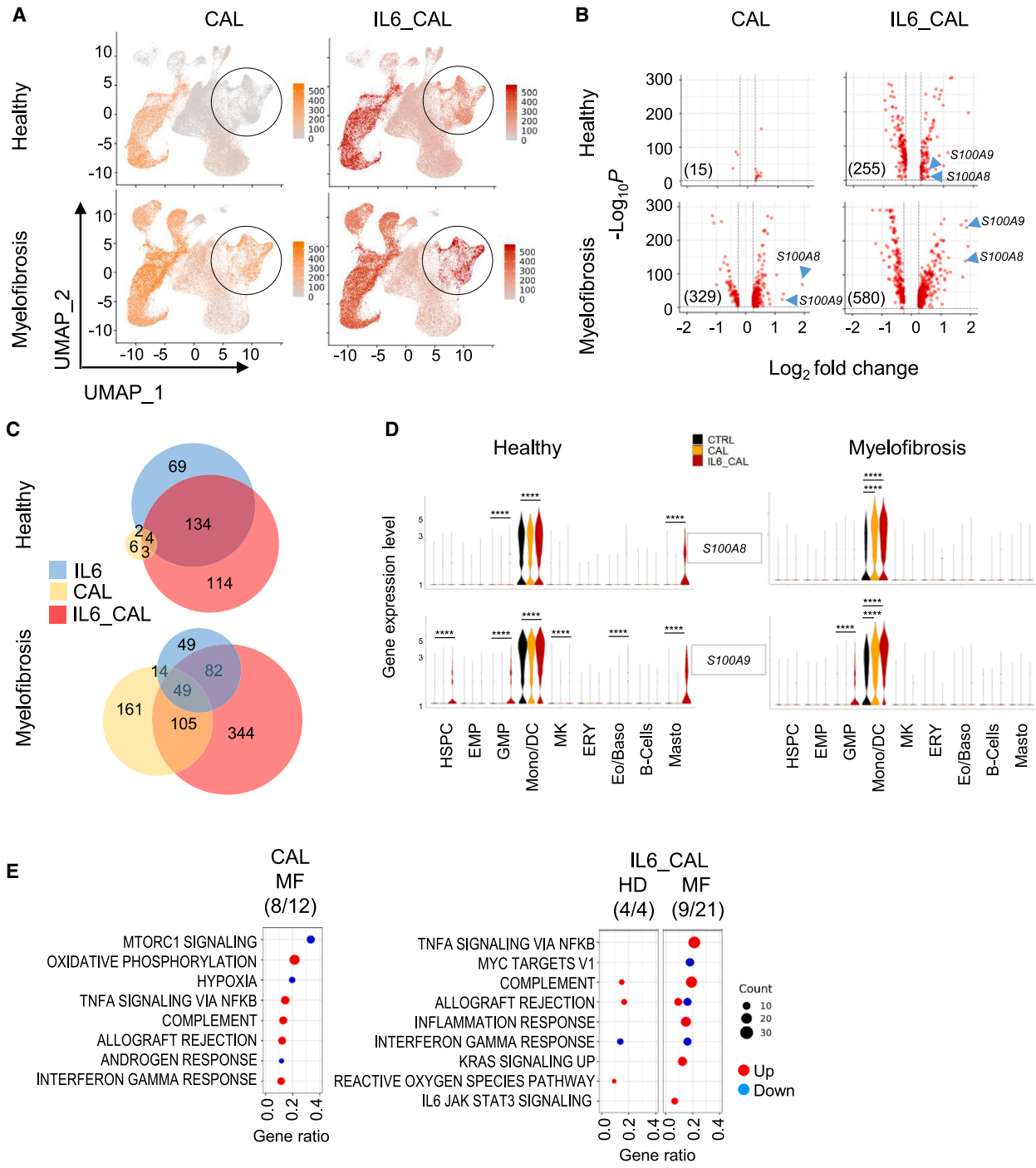

Figure 3. The effects of calprotectin on monocytes are restricted to MF-derived samples

(A) UMAP visualization of DEGs in the healthy donor (HD) and primary myelofibrosis (MF) samples after 7 days of treatment with CAL or IL6_CAL; circles indicate the Mo/DC cluster.

(B) Volcano plots of DEGs in Mos/DCs generated from HD and MF patient CD34^{+} cells upon treatment with CAL or IL6_CAL; the total number of significant DEGs indicated between comas.

(C) Venn diagram of DEG numbers and overlaps in the Mo/DC cluster generated by HD and MF cells treated with CAL (yellow), IL6 (blue), and IL6_CAL (red).

(D. Violin plot of *S100A8* and *S100A9* gene expression in the 9 cell populations generated by HD and MF CD34^{+} cells without (black) and with CAL (orange) or IL6_CAL (red); Unpaired Wilcoxon rank-sum test; **** padj<10^{-3}.

(E) Pathway analysis in HD and MF cell-derived Mo/DC population, based on DEGs (upregulated in red, downregulated in blue) depicted in panel B. See also Figure S4.

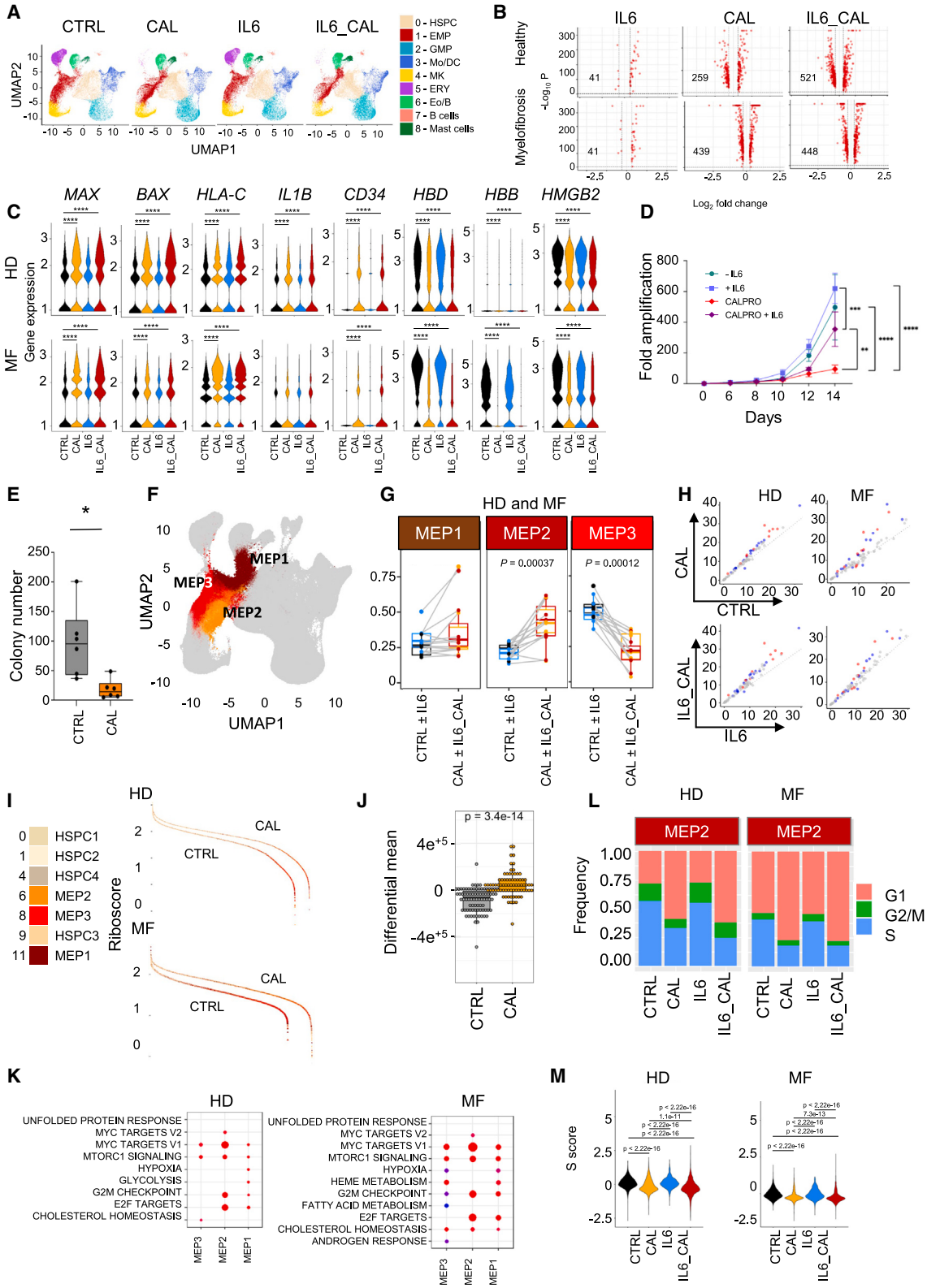

(legend on next page)

observed with IL6 alone (n = 194, Figure 2C), with IL6_CAL specifically affecting the expression of 344 genes (Figure 3C). Together, CAL reorganizes gene expression in Mo/DCs derived from MF CD34$^+$ cells but has no or limited effects on Mo/DCs derived from HD CD34$^+$ cells.

The *S100A8* and *S100A9* genes were among the genes whose expression was promoted by CAL in Mo/DCs generated from MF CD34$^+$ cells (Figures 3B and 3D). Higher resolution confirmed the response of MF cell-derived immature monocytes to CAL ± IL6 (Figures S4B and S4C). Oxidative phosphorylation was the main pathway activated by CAL alone in MF cell-derived Mo/DCs, while the IL6_CAL combination activated also several inflammatory pathways in these cells (Figure 3E). Together, CAL promotes the generation, by MF CD34$^+$ cells, of Mo/DCs exhibiting a proinflammatory transcriptome, including overexpression of *S100A8* and *S100A9* genes, an effect amplified by the combination of CAL with IL6.

This observation suggested that a feedforward loop may amplify the effects of CAL on MF pathology. The high level of CAL already present in the medium precluded the detection of a significant increase in CAL in the supernatant of cells cultured with IL6_CAL, as detected with IL6 alone (Figure 2I). We observed an increase in the production of IL16, CXCL13, and CXCL16, as with IL6 alone (Figure 2I), and further detected an increase in the production of CCL3 and CXCL8 (Figure S4D).

Calprotectin inhibits erythroid cell differentiation at the progenitor level

In contrast with HD CD34$^+$ cells, JAK2-V617F CD34$^+$ cells generated erythroid cells (Figure 2A) after 7 days in liquid culture. This erythropoietin (EPO)-independent erythropoiesis was inhibited by CAL, an effect also observed when IL6 was associated with CAL but not with IL6 alone (Figures 4A and S5A). CAL increased the expression of 259 genes in HD cell-derived MEPs, and this effect was amplified in JAK2-V617F cell derived MEPs (Figure 4B).

Using Human Phenotype Ontology (HPO) gene sets and focusing on hematopoiesis-related terms, DEGs related to anemia were the main clinical manifestation of the effects of CAL on MEPs (Figure S5B). The expression of most genes modulated by CAL ± IL6 in MEPs generated by HD CD34$^+$ cells was modulated also in MEPs generated by MF CD34$^+$ cells (Figures 4C, S5C and S5D; Table S3). ORA of the hallmark pathway indicated the downregulation of the cell cycle and mTORC1 signaling pathways in MEPs generated in the presence of CAL, while the inflammatory response and p53 pathways were activated in these cells.

To confirm the effects of CAL on erythroid differentiation, we performed a liquid culture of healthy adult and cord blood CD34$^+$ cells in the presence of EPO.[19] CAL reproducibly prevented the proliferation of cells undergoing terminal erythroid differentiation (Figure 4D). This inhibitory effect of CAL on erythroid progenitor expansion was confirmed by testing the ability of erythroid-biased cells expanded in the presence of SCF and EPO and collected on day 5 of liquid culture to generate colonies in semisolid medium (Figures 4E, S5E, and S5F).

Analysis of the MEP compartment at a higher resolution distinguished three MEP subsets (Figure 4F). Within these subsets, CAL ± IL6 provoked a significant increase in the fraction of MEP2 (Figure 4G).

The dysregulated gene sets associated with anemia in the MEP2 subset included an overrepresentation of ribosomal protein-encoding genes (Table S4). We previously demonstrated how crucial the timing of ribosome biogenesis downregulation was for terminal erythroid differentiation.[19,20] Upon exposure to CAL ± IL6, the genes encoding short and long ribosomal proteins (RPS and RPL, respectively) remained highly expressed in MEP2 cells compared to untreated or IL6-treated samples, without an

Figure 4. Calprotectin inhibits red cell differentiation at the MEP level

(A) UMAP of cells generated by *ex vivo* culture of MF CD34$^+$ cells in the absence (CTRL) or presence of CAL, IL-6, and IL6_CAL.

(B) Volcano plot of DEGs analyzed in cluster 1 (MEP) generated from HD and MF CD34$^+$ cells upon the indicated treatment compared to untreated samples. The numbers of DEGs are indicated.

(C) Expression of selected genes significantly modified by CAL alone or combined with IL6 in the MEP cluster generated from HD or MF cells (Unpaired Wilcoxon rank-sum test, **** padj<0.0001).

(D) Effect of CAL on the number of BFU-E generated by cells collected on day 4 of culture in the presence of EPO and the indicated cytokines (n = 6, mean ± SEM, two-way ANOVA, **p < 0.01; ***p < 0.001; ***p < 0.0001).

(E) Inhibitory effect of CAL on the number of cells generated by CD34$^+$ cord blood cells in the presence of EPO (n = 6, median [min-max], paired Wilcoxon test, *p < 0.05).

(F) Visualization of three MEP subtypes, from MEP1 to MEP3, identified at higher resolution.

(G) Fraction of MEP1, MEP2, and MEP3 among total MEPs in HD and MF samples treated with CAL ± IL6 compared to samples that remained untreated or were treated with IL6 alone (CTRL ± IL6); paired Wilcoxon test.

(H) Impact of indicated cytokines on the expression of genes encoding the small (RPS) and the large (RPL) subunits of ribosomal proteins (RP) in MEP2. Upper panel, CAL vs. CTRL; lower panel, IL6_CAL vs. IL6. Each point is the mean expression of a ribosomal protein-encoding gene in a given treatment condition. The color points indicate genes whose expression was significantly modified (RPS, red; RPL, blue). The gray points indicate RP genes whose expression did not significantly change according to the differential expression analysis.

(I) Ribosome scores of the healthy donor (HD) and myelofibrosis (MF) samples from untreated (CTRL) and calprotectin-treated (CAL) cells, as measured using Seurat's AddModuleScore function for RPL and RPS genes shown on 4H. On the x axis, the cells are sorted by their ribosome score (shown on the y axis) and colored according to their cluster identity.

(J) Validation of the impact of CAL on RP through proteomic analysis of erythroid cells generated in the presence of EPO ± CAL. For each detected RP (n = 81), the mean expression level on day 12 was subtracted from the mean expression on day 15; unpaired Wilcoxon rank-sum test.

(K) Comparison of overrepresented pathways identified downregulated DEGs in MEP1, MEP2, and MEP3 cells generated from HD or MF samples upon treatment with CAL.

(L) Cell cycle impact of cytokine treatment on the cell cycle repartition of MEP2 cells from healthy donors and myelofibrosis.

(M) Seurat S score in MEP2 from HD and MF CD34$^+$ cells under the indicated treatment; unpaired Wilcoxon rank-sum test. See also Figure S5.

imbalance between *RPS*- and *RPL*-encoding genes (Figure 4H). We scored the expression of 88 *RPS* and *RPL* genes in the HSPC and MEP clusters. These riboscores indicated that CAL delayed the decrease in *RP* gene expression that typically precedes terminal stages of erythroid differentiation (Figures 4I and S4G).

To validate this observation, we performed a proteomic analysis of erythroid precursors generated in liquid culture in the presence of EPO, without and with CAL. CAL prevented the decrease of the majority of RPs detected between day 12 and day 15 of the culture (Figure 4J).

CAL-induced perturbation of RP gene downregulation in MEPs could induce ribosomal stress and alter cell cycle progression. Accordingly, ORA of genes downregulated in MEP subsets generated by HD CD34$^+$ cells upon CAL exposure revealed changes in cell cycle regulatory pathways that predominated in MEP2 and were amplified in those generated by JAK2-V617F CD34$^+$ cells (Figures 4K, 4L, and S5H). CAL ± IL6 increased the proportion of MEP2 cells in the G1 phase (Figure 4L), which was validated by a decreased S score (Figure 4M).

Together, CAL inhibits erythroid cell differentiation by inducing the accumulation of an MEP subset in the G1 phase of the cell cycle. Analysis of multiple stress signatures in MEP2 cells revealed a diapause-like signature[21] as the most significantly modulated by CAL ± IL6 (Figure S5I).

Calprotectin rewires gene expression in megakaryocytes

UMAP visualization of DEGs on day 7 indicated that both CAL (Figure 3A) and IL6 (Figure 2B) could also modulate gene expression in MKs on day 7 of liquid culture. MKs are major players in both severe inflammation[22] and MF pathophysiology.[23] CAL ± IL6 decreased the fraction of MKs generated by HD and MF CD34$^+$ cells (Figure 5A). The number of genes whose expression was modulated in MKs was greater in the presence of CAL (Figures 5B and 5C), and a strong overlap was observed between genes modulated by CAL and IL6_CAL (Figures 5C and S6A). As in the MEPs, CAL activated the inflammatory and p53 pathways while decreasing the cell cycle and mTORC1 signaling pathways in MKs (Figures 5D and S6B).

Recent evidence indicates that while the majority of MKs arise via a shared trajectory with the erythroid lineage, some HSCs could be primed to become MKs in both HDs[24] and patients with MF.[25] Analysis of time-resolved differentiation trajectories using slingshot revealed a small subset of MKs with a low pseudotime, suggesting that these cells could have emerged directly from the HSPC population (Figure 5E). Quantification revealed a significant increase in this MK fraction in the presence of IL6, which was amplified by CAL (Figure 5F). Overall, CAL decreases the fraction of MKs generated through MEPs but promotes the differentiation of MK-biased HSCs in combination with IL6.

Identification of the calprotectin signature under pathological conditions

To determine the relevance of these results in human diseases, we generated three signatures. The first, established by using the Seurat FindAllMarkers function, included 110 genes that identify MEP2-like cells (Table S5). The two other signatures included genes that were similarly modulated in HD and MF CD34$^+$ cell-derived MEP2 cells and included 108 upregulated genes (CAL-up signature) and 150 downregulated genes (CAL-down signature) (Figure 6A and Table S6).

We collected scRNA-seq data generated from bone marrow cells of patients with mild (n = 3) or severe (n = 4) COVID-19[26] and used the first signature to identify MEP2-like cells (Figure S7A). We then examined the CAL-up and CAL-down signatures in these cells. The CAL-up gene score was significantly greater in the MEP2-like cells of patients with severe COVID-19 than in those with mild COVID-19, while the CAL-down signature score was significantly lower (Figures 6B and S6A).

We then looked for these signatures in the scRNA-seq data collected from patients with myeloid malignancies. As monocytes are one of the main cell populations producing CAL *in vivo*, we reasoned that the CAL signatures in patient bone marrow-derived MEP2-like cells could depend on monocyte count. We tested this hypothesis via the scRNA-seq of bone marrow CD34$^+$ cells collected from patients with MF (25). Having identified MEP2-like cells (Figure S7B), we separated patients without (N = 10) and with (N = 5) peripheral blood monocytosis (cutoff, 1G/L) and observed an association between this parameter and the CAL-up ($p = 3.3e^{-11}$) and CAL-down ($p = 7.2e^{-5}$) signatures in MEP-2-like cells (Figure 6C).

The same analysis was performed on scRNA-seq data generated from bone marrow CD34$^+$ cells of patients with chronic myelomonocytic leukemia (CMML).[27] As these patients exhibit monocytosis by definition, we separated those with very high monocyte counts (≥6 G/L, N = 8) from those with monocyte counts between 1 and 6G/L (N = 23), again finding that the CAL-up and CAL-down signatures in MEP2-like cells (Figure S7C) were associated with higher monocyte counts (Figure 6D). The same observation was made also when testing white blood cell count with a cutoff of 13 G/L, which separates dysplastic and proliferative patients with CMML according to the WHO classification (Figure S7D).[28] Since hemoglobin levels were available in this dataset, we could observe that CAL-up and CAL-down signatures were significantly different in 14 patients with CMML whose hemoglobin levels were ≤100 g/L compared to 25 patients with hemoglobin >100 g/L (Figure 6E).

Finally, we searched for CAL-up and CAL-down signatures in bulk RNA-seq data of acute myeloid leukemia (AML) samples.[29] As we did not obtain the absolute number of circulating monocytes, we separated patients with low (<10%; n = 171) and high (≥10%; n = 100) monocyte fractions among WBCs, revealing an association between CAL signatures and higher monocyte fractions (Figure 6E).

Together, CAL signatures identified in MEP2 cells generated *ex vivo* can be detected in the bone marrow cells of patients with severe infection or a myeloid malignancy, correlating with the amount of generated monocytes.

DISCUSSION

CAL is increasingly being recognized as an important mediator of systemic inflammation. We show here that the S100A8/S100A9 heterodimer, whose production by monocytes is amplified by IL6, contributes to erythropoiesis suppression. In various

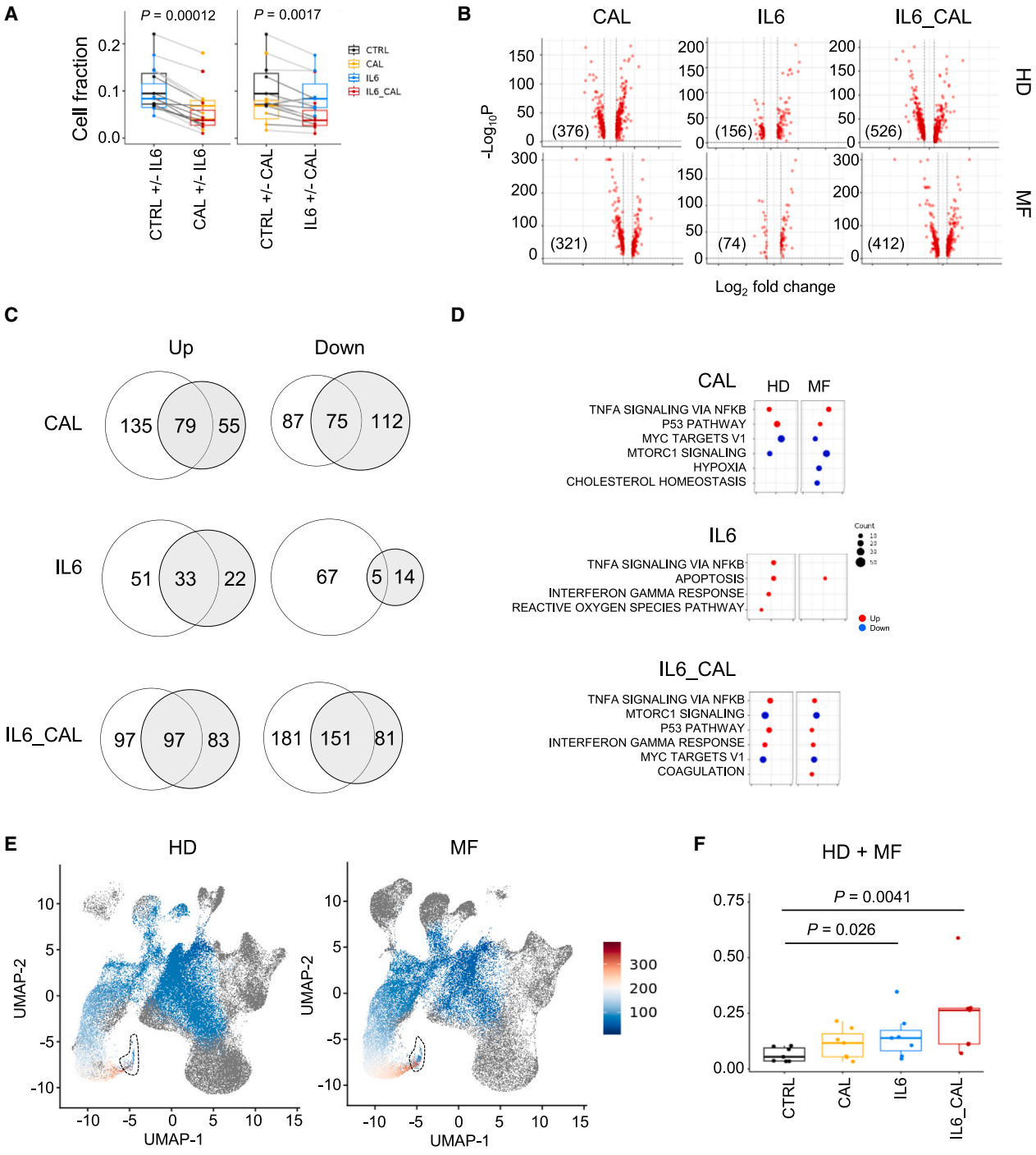

Figure 5. CAL rewires gene expression in megakaryocytes

(A) Cytokine impact on the fraction of MKs among cells generated by HD CD34$^+$ cells in the presence of the indicated cytokines. The left panel shows the effects of CAL; the right panel shows the effects of IL6; black, untreated CTRL; orange, CAL alone; blue, IL6 alone; red, IL6_CAL; statistical test: paired Wilcoxon test.

(B) Volcano plot representation of DEGs identified in MKs (low-resolution UMAP, cluster 4) under the indicated treatments of HD and MF CD34$^+$ cells; the total number of DEGs in every condition is indicated.

(C) Proportional Venn diagram of up- and downregulated genes (numbers) in HD (white) and MF (gray) samples.

(D) Pathway analysis of upregulated (red) and downregulated (blue) genes in HD and MF samples. The top significant pathways are plotted.

(E) Trajectory analysis using slingshot in HD and MF samples; UMAP colored according to the pseudotime of the MK differentiation lineage.

(F) MK fraction directly generated by HSPCs in HD and MF samples treated as indicated. Statistical test: paired Wilcoxon test. See also Figure S6.

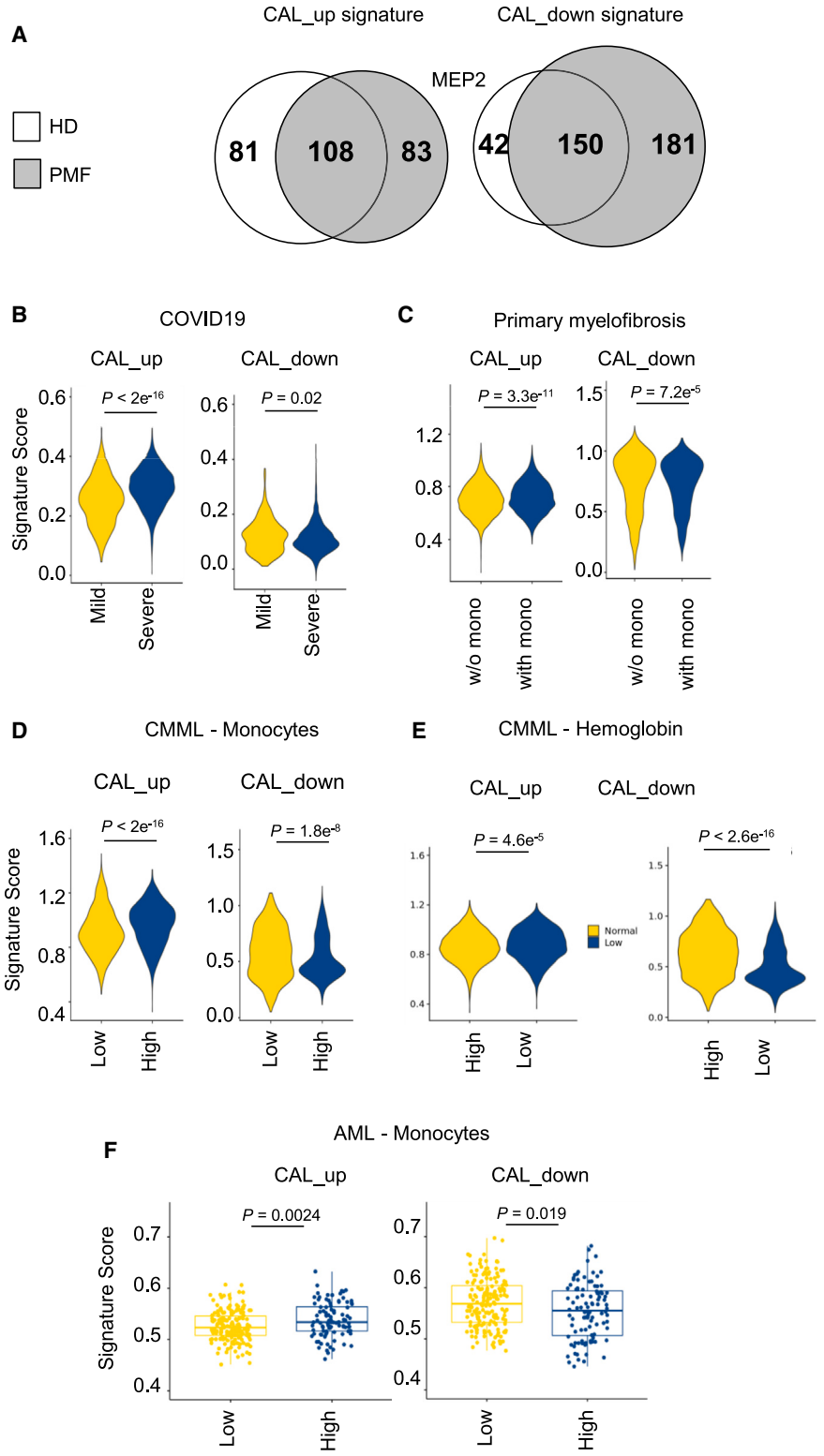

Figure 6. Calprotectin signatures in MEPs across hematopoietic diseases

(A) Proportional Venn diagram used to generate CAL_up (left) and CAL_down (right) signatures, based on DEGs in MEP2 generated from HD cells without and with CAL.

(legend continued on next page)

pathological situations, the signature of CAL effects can be detected in erythroid progenitors and correlates with monocyte amplification.

In the context of the JAK2-V617F mutation, CAL also promotes the generation of proinflammatory monocytes that overexpress the *S100A8* and *S100A9* genes. This later observation suggests a feedforward loop that may amplify the hematopoietic reaction to inflammatory stress in patients with a myeloproliferative neoplasm.

IL6 acts synergistically with FLT3L and SCF to promote hematopoietic cell expansion.[14,30] Our study demonstrated that, in early human hematopoietic cells, IL6 is a trigger of *S100A8* and *S100A9* gene expression that increases within a few hours in $CD34^+$ cells and predominates after 7 days in maturing monocytes. A similar promotion of CAL secretion by IL6 was depicted in other cell types, e.g., in breast cancer cells.[31]

The increased chromatin accessibility of a monocyte-specific enhancer that is common to the *S100A8* and *S100A9* genes argues for the role of epigenetic features in the modulation of their expression.[18] In contrast, CAL has no impact on IL6 production by hematopoietic progenitors. CAL-induced activation of oxidative phosphorylation and metabolic pathways indicates that $CD34^+$ HSPCs sense extracellular CAL.[32,33] While chronic exposure to CAL produced by mesenchymal stromal cells of the bone marrow environment could drive genotoxic stress through p53-S100A8/9-TLR inflammatory signaling in HSPCs,[32] the initial response of HSPCs to CAL is limited compared to that to acute exposure to IL6.

The main effect of CAL was identified after 7 days in culture. CAL restricts both the EPO-dependent erythroid maturation of healthy $CD34^+$ cells and the EPO-independent maturation of JAK2-V617F $CD34^+$ cells, generating a diapause-like signature in MEPs.[21,34] CAL was involved in erythropoiesis inhibition in a mouse model of del(5q) myelodysplastic neoplasm in which the inactivation of the *Rps14* gene increases the expression of the *S100a8* gene in erythroid precursors, triggering a p53-mediated erythroid differentiation defect through cell-intrinsic and cell-extrinsic mechanisms that involve CAL.[35]

The delay in RP gene downregulation,[19] which is under the control of the mTORC1 signaling pathway,[36] could account for erythropoiesis perturbation induced by CAL, potentially contributing to the decrease in cell cycle speed[37] that may contribute to inhibiting erythroid differentiation.[38]

IL6 is an essential but indirect regulator of anemia caused by inflammation, acting by increasing hepcidin production by hepatocytes through the JAK2/STAT3 pathway.[39] Our results identified another indirect contribution of IL6 to anemia-related inflammation through the promotion of CAL secretion by maturing monocytes, positioning CAL as an IL6 amplifier.[40]

In the context of JAK2-V617F, not only does CAL inhibit the EPO-independent generation of erythroid cells but also this cytokine promotes the generation of proinflammatory monocytes that overexpress the *S100A8* and *S100A9* genes. Alarmins are a driving force for the development of hematopoietic malignancies. These mediators promote myelodysplastic neoplasm-associated cytopenias through the expansion of myeloid-derived suppressive cells[41] and the activation of the NLRP3 inflammasome in hematopoietic progenitors.[42] In the context of myeloproliferative neoplasms, the overexpression of the *S100A8* and *S100A9* genes in hematopoietic progenitors reflects disease evolution,[43] while their expression in niche cells demarcates the fibrotic progression of JAK2-V617F neoplasms.[32,44] A gene signature of the effects of CAL was detected in bone marrow erythroid progenitors of patients with a chronic myeloid malignancy. CAL produced by stromal cells of the bone marrow niche was shown to promote MF.[44] We show here that the CAL signature correlates also with monocyte count whose elevation is a negative prognostic factor in this disease.[45,46] The hyper-reactivity of monocytes generated from MF $CD34^+$ cells to CAL, probably driven by JAK2-V617F mutation amplifying the signaling response to inflammatory cytokines, might contribute to the increased severity of systemic inflammatory diseases such as COVID-19 in patients with MF and other hematological malignancies.[15,16] The CAL signature also correlates with monocyte count in chronic myelomonocytic leukemia[47] in which the potential contribution of CAL to the worse outcome of disease proliferative subtype deserves to be explored.

Together, this work identifies a new mechanism by which IL6 promotes anemia in the context of systemic inflammation,[48] i.e., IL6 generates monocytes that overproduce CAL that, in turn, inhibits erythropoiesis at the level of progenitors. This detrimental role of CAL is amplified in the context of pathological hematopoiesis. CAL could bind multiple receptors on the surface of the cells.[49] In addition to TLR4, bioinformatic analysis of cell-cell interactions in scRNAseq data using LIANA (LIgand-receptor ANalysis framework) package[50] suggested a possible interaction with CD36. Interestingly, CD36-expressing MEP disappears in CAL-treated samples. Identifying the receptor(s) and signaling pathways involved in erythroid differentiation inhibition and JAK2-V617F monocyte response to CAL may suggest therapeutic strategies to modulate CAL effects during systemic inflammation, as already tested in the context of myelofibrosis.[44]

Limitations of the study

In the tested *ex vivo* experimental settings, the amount of calprotectin released by monocytes in the culture medium within 7 days is not sufficient to reach the concentrations measured in the circulating plasma of patients with sepsis or a severe myeloid malignancy, which are needed to inhibit erythroid differentiation. The influence of sex and gender on the described pathways could not be explored as most available samples were

(B–E) Score of CAL_up and CAL_down signatures in MEP2-like cells collected from scRNAseq performed in bone marrow cells collected from (B) Patients with mild (yellow) and severe (blue) COVID-19. (C) Primary myelofibrosis without (yellow) and with (blue) peripheral blood monocytosis (cutoff 1 G/L). (D) Chronic myelomonocytic leukemia with very high (blue) and high peripheral blood monocytosis (cutoff, 6 G/L). (E) Chronic myelomonocytic leukemia without (yellow) and with (blue) low hemoglobin level (cutoff, 100 g/L).

(F) Score of the CAL_up and CAL_down signatures in bulk RNA-seq of acute myeloid leukemia cells from patients without (yellow) and with (blue) an elevated fraction of peripheral blood monocytes (cutoff 10% of the WBC count). All statistical analyses: Wilcoxon unpaired test. See also Figure S7.

collected from males. Another limitation of the experimental system is the lack of mature granulocytes that may contribute *in vivo* to the synthesis and secretion of calprotectin in inflammatory conditions. Animal models might be needed to validate the contribution of calprotectin secreted by mature myeloid cells to inflammatory anemia.

RESOURCE AVAILABILITY

Lead contact

Requests for further information and resources should be directed to and will be fulfilled by the lead contact, Eric Solary, INSERM U1287, Gustave Roussy Cancer Center, 114 rue Edouard Vaillant, F-94805, Villejuif, France. eric.solary@gustaveroussy.fr.

Materials availability

This study did not generate new unique reagents.

Data and code availability

- Standardized scRNAseq data are deposited at the EGA public data repository and are publicly available as of the date of publication. Accession numbers are listed in the key resources table."
- The mass spectrometry proteomics data have been deposited to the ProteomeXchange Consortium via the PRIDE partner repository. The dataset identifier is listed in the key resources table.
- This article does not report the original code.

ACKNOWLEDGMENTS

This work was funded by the Agence Nationale de la Recherche (ANR). The team is labeled by the Ligue Nationale Contre le Cancer (F.P.). V.M. was supported by PhD grants from the French Ministry of Research and Higher Education and the Foundation ARC. We are grateful to the biological platforms of Gustave Roussy (Philippe Rameau, Imaging and cytometry; N.D., Fundamental genomics) and Cochin Institute (Muriel Andrieu, Cybio; Marjorie Leduc, Proteom'ic).

AUTHOR CONTRIBUTIONS

E.S. Conceptualization, methodology, validation; formal analysis; investigation resources; data curation; and writing – original draft preparation; V.M. performed most of the biological experiments, L.L., V.M, and M.A. performed computational analyses and data curation, N.D. performed sequencing and ATAC-seq analyses, F.Pa. and W.V. provided biological samples, V.M., L.L., I.P., L.V., A.S., F.Po., W.V., D.S.B., H.R., V.M., and J.J.D. analyzed the data, M.F. performed erythroid cell cultures and analyzed the data, E.S. designed the study, analyzed the data and wrote the article, all authors reviewed and approved the article.

DECLARATION OF INTERESTS

The authors declare no competing interest.

STAR★METHODS

Detailed methods are provided in the online version of this paper and include the following:

SUPPLEMENTAL INFORMATION

Supplemental information can be found online at https://doi.org/10.1016/j.isci.2024.111522.

Received: June 20, 2024
Revised: October 2, 2024
Accepted: November 29, 2024
Published: December 2, 2024

REFERENCES

1. Medzhitov, R. (2021). The spectrum of inflammatory responses. Science *374*, 1070–1075. https://doi.org/10.1126/science.abi5200.
2. Chan, J.K., Roth, J., Oppenheim, J.J., Tracey, K.J., Vogl, T., Feldmann, M., Horwood, N., Nanchahal, J., and Nanchahal, J. (2012). Alarmins: awaiting a clinical response. J. Clin. Invest. *122*, 2711–2719. https://doi.org/10.1172/JCI62423.
3. Vogl, T., Leukert, N., Barczyk, K., Strupat, K., and Roth, J. (2006). Biophysical characterization of S100A8 and S100A9 in the absence and presence of bivalent cations. Biochim. Biophys. Acta *1763*, 1298–1306. https://doi.org/10.1016/j.bbamcr.2006.08.028.
4. Pruenster, M., Vogl, T., Roth, J., and Sperandio, M. (2016). S100A8/A9: From basic science to clinical application. Pharmacol. Ther. *167*, 120–131. https://doi.org/10.1016/j.pharmthera.2016.07.015.
5. Edgeworth, J., Gorman, M., Bennett, R., Freemont, P., and Hogg, N. (1991). Identification of p8,14 as a highly abundant heterodimeric calcium binding protein complex of myeloid cells. J. Biol. Chem. *266*, 7706–7713.
6. Vogl, T., Tenbrock, K., Ludwig, S., Leukert, N., Ehrhardt, C., van Zoelen, M.A.D., Nacken, W., Foell, D., van der Poll, T., Sorg, C., and Roth, J. (2007). Mrp8 and Mrp14 are endogenous activators of Toll-like receptor 4, promoting lethal, endotoxin-induced shock. Nat. Med. *13*, 1042–1049. https://doi.org/10.1038/nm1638.
7. Takizawa, H., and Manz, M.G. (2017). Impact of inflammation on early hematopoiesis and the microenvironment. Int. J. Hematol. *106*, 27–33. https://doi.org/10.1007/s12185-017-2266-5.
8. Sreejit, G., Abdel-Latif, A., Athmanathan, B., Annabathula, R., Dhyani, A., Noothi, S.K., Quaife-Ryan, G.A., Al-Sharea, A., Pernes, G., Dragoljevic, D., et al. (2020). Neutrophil-Derived S100A8/A9 Amplify Granulopoiesis After Myocardial Infarction. Circulation *141*, 1080–1094. https://doi.org/10.1161/CIRCULATIONAHA.119.043833.
9. Zhao, J.L., Ma, C., O'Connell, R.M., Mehta, A., DiLoreto, R., Heath, J.R., and Baltimore, D. (2014). Conversion of danger signals into cytokine signals by hematopoietic stem and progenitor cells for regulation of stress-induced hematopoiesis. Cell Stem Cell *14*, 445–459. https://doi.org/10.1016/j.stem.2014.01.007.
10. Chapuis, N., Ibrahimi, N., Belmondo, T., Goulvestre, C., Berger, A.E., Mariaggi, A.A., Andrieu, M., Chenevier-Gobeaux, C., Bayle, A., Campos, L., et al. (2022). Dynamics of circulating calprotectin accurately predict the outcome of moderate COVID-19 patients. EBioMedicine *80*, 104077. https://doi.org/10.1016/j.ebiom.2022.104077.
11. Silvin, A., Chapuis, N., Dunsmore, G., Goubet, A.G., Dubuisson, A., Derosa, L., Almire, C., Hénon, C., Kosmider, O., Droin, N., et al. (2020). Elevated Calprotectin and Abnormal Myeloid Cell Subsets Discriminate

Severe from Mild COVID-19. Cell *182*, 1401–1418.e18. https://doi.org/10.1016/j.cell.2020.08.002.

12. Schulte-Schrepping, J., Reusch, N., Paclik, D., Baßler, K., Schlickeiser, S., Zhang, B., Krämer, B., Krammer, T., Brumhard, S., Bonaguro, L., et al. (2020). Severe COVID-19 Is Marked by a Dysregulated Myeloid Cell Compartment. Cell *182*, 1419–1440.e23. https://doi.org/10.1016/j.cell.2020.08.001.
13. Wang, X., Wen, Y., Xie, X., Liu, Y., Tan, X., Cai, Q., Zhang, Y., Cheng, L., Xu, G., Zhang, S., et al. (2021). Dysregulated hematopoiesis in bone marrow marks severe COVID-19. Cell Discov. *7*, 60. https://doi.org/10.1038/s41421-021-00296-9.
14. Bernad, A., Kopf, M., Kulbacki, R., Weich, N., Koehler, G., and Gutierrez-Ramos, J.C. (1994). Interleukin-6 is required *in vivo* for the regulation of stem cells and committed progenitors of the hematopoietic system. Immunity *1*, 725–731. https://doi.org/10.1016/s1074-7613(94)80014-6.
15. Reyes, M., Filbin, M.R., Bhattacharyya, R.P., Sonny, A., Mehta, A., Billman, K., Kays, K.R., Pinilla-Vera, M., Benson, M.E., Cosimi, L.A., et al. (2021). Plasma from patients with bacterial sepsis or severe COVID-19 induces suppressive myeloid cell production from hematopoietic progenitors *in vitro*. Sci. Transl. Med. *13*, eabe9599. https://doi.org/10.1126/scitranslmed.abe9599.
16. Landtblom, A.R., Andersson, T.M.L., Dickman, P.W., Smedby, K.E., Eloranta, S., Batyrbekova, N., Samuelsson, J., Björkholm, M., and Hultcrantz, M. (2021). Risk of infections in patients with myeloproliferative neoplasms-a population-based cohort study of 8363 patients. Leukemia *35*, 476–484. https://doi.org/10.1038/s41375-020-0909-7.
17. Vijenthira, A., Gong, I.Y., Fox, T.A., Booth, S., Cook, G., Fattizzo, B., Martín-Moro, F., Razanamahery, J., Riches, J.C., Zwicker, J., et al. (2020). Outcomes of patients with hematologic malignancies and COVID-19: a systematic review and meta-analysis of 3377 patients. Blood *136*, 2881–2892. https://doi.org/10.1182/blood.2020008824.
18. Jauch-Speer, S.L., Herrera-Rivero, M., Ludwig, N., Véras De Carvalho, B.C., Martens, L., Wolf, J., Imam Chasan, A., Witten, A., Markus, B., Schieffer, B., et al. (2022). C/EBPδ-induced epigenetic changes control the dynamic gene transcription of S100a8 and S100a9. Elife *11*, e75594. https://doi.org/10.7554/eLife.75594.
19. Le Goff, S., Boussaid, I., Floquet, C., Raimbault, A., Hatin, I., Andrieu-Soler, C., Salma, M., Leduc, M., Gautier, E.F., Guyot, B., et al. (2021). p53 activation during ribosome biogenesis regulates normal erythroid differentiation. Blood *137*, 89–102. https://doi.org/10.1182/blood.2019003439.
20. Gautier, E.F., Ducamp, S., Leduc, M., Salnot, V., Guillonneau, F., Dussiot, M., Hale, J., Giarratana, M.C., Raimbault, A., Douay, L., et al. (2016). Comprehensive Proteomic Analysis of Human Erythropoiesis. Cell Rep. *16*, 1470–1484. https://doi.org/10.1016/j.celrep.2016.06.085.
21. Rehman, S.K., Haynes, J., Collignon, E., Brown, K.R., Wang, Y., Nixon, A.M.L., Bruce, J.P., Wintersinger, J.A., Singh Mer, A., Lo, E.B.L., et al. (2021). Colorectal Cancer Cells Enter a Diapause-like DTP State to Survive Chemotherapy. Cell *184*, 226–242.e21. https://doi.org/10.1016/j.cell.2020.11.018.
22. Bernardes, J.P., Mishra, N., Tran, F., Bahmer, T., Best, L., Blasé, J.I., Bordoni, D., Franzenburg, J., Geisen, U., Josephs-Spaulding, J., et al. (2020). Longitudinal Multi-omics Analyses Identify Responses of Megakaryocytes, Erythroid Cells, and Plasmablasts as Hallmarks of Severe COVID-19. Immunity *53*, 1296–1314.e9. https://doi.org/10.1016/j.immuni.2020.11.017.
23. Duparc, H., Muller, D., Gilles, L., Chédeville, A.L., El Khoury, M., Guignard, R., Debili, N., Wittner, M., Kauskot, A., Pasquier, F., et al. (2024). Deregulation of the p19/CDK4/CDK6 axis in Jak2(V617F) megakaryocytes accelerates the development of myelofibrosis. Leukemia *38*, 898–902. https://doi.org/10.1038/s41375-024-02170-5.
24. Yamamoto, R., Morita, Y., Ooehara, J., Hamanaka, S., Onodera, M., Rudolph, K.L., Ema, H., and Nakauchi, H. (2013). Clonal analysis unveils self-renewing lineage-restricted progenitors generated directly from hematopoietic stem cells. Cell *154*, 1112–1126. https://doi.org/10.1016/j.cell.2013.08.007.
25. Psaila, B., Wang, G., Rodriguez-Meira, A., Li, R., Heuston, E.F., Murphy, L., Yee, D., Hitchcock, I.S., Sousos, N., O'Sullivan, J., et al. (2020). Single-Cell Analyses Reveal Megakaryocyte-Biased Hematopoiesis in Myelofibrosis and Identify Mutant Clone-Specific Targets. Mol. Cell *78*, 477–492.e8. https://doi.org/10.1016/j.molcel.2020.04.008.
26. Cheong, J.G., Ravishankar, A., Sharma, S., Parkhurst, C.N., Grassmann, S.A., Wingert, C.K., Laurent, P., Ma, S., Paddock, L., Miranda, I.C., et al. (2023). Epigenetic memory of coronavirus infection in innate immune cells and their progenitors. Cell *186*, 3882–3902.e24. https://doi.org/10.1016/j.cell.2023.07.019.
27. Ferrall-Fairbanks, M.C., Dhawan, A., Johnson, B., Newman, H., Volpe, V., Letson, C., Ball, M., Hunter, A.M., Balasis, M.E., Kruer, T., et al. (2022). Progenitor Hierarchy of Chronic Myelomonocytic Leukemia Identifies Inflammatory Monocytic-Biased Trajectory Linked to Worse Outcomes. Blood Cancer Discov. *3*, 536–553. https://doi.org/10.1158/2643-3230.BCD-21-0217.
28. Khoury, J.D., Solary, E., Abla, O., Akkari, Y., Alaggio, R., Apperley, J.F., Bejar, R., Berti, E., Busque, L., Chan, J.K.C., et al. (2022). The 5th edition of the World Health Organization Classification of Haematolymphoid Tumours: Myeloid and Histiocytic/Dendritic Neoplasms. Leukemia *36*, 1703–1719. https://doi.org/10.1038/s41375-022-01613-1.
29. Bottomly, D., Long, N., Schultz, A.R., Kurtz, S.E., Tognon, C.E., Johnson, K., Abel, M., Agarwal, A., Avaylon, S., Benton, E., et al. (2022). Integrative analysis of drug response and clinical outcome in acute myeloid leukemia. Cancer Cell *40*, 850–864.e9. https://doi.org/10.1016/j.ccell.2022.07.002.
30. Peters, M., Schirmacher, P., Goldschmitt, J., Odenthal, M., Peschel, C., Fattori, E., Ciliberto, G., Dienes, H.P., Meyer zum Büschenfelde, K.H., and Rose-John, S. (1997). Extramedullary expansion of hematopoietic progenitor cells in interleukin (IL)-6-sIL-6R double transgenic mice. J. Exp. Med. *185*, 755–766. https://doi.org/10.1084/jem.185.4.755.
31. Rodriguez-Barrueco, R., Yu, J., Saucedo-Cuevas, L.P., Olivan, M., Llobet-Navas, D., Putcha, P., Castro, V., Murga-Penas, E.M., Collazo-Lorduy, A., Castillo-Martin, M., et al. (2015). Inhibition of the autocrine IL-6-JAK2-STAT3-calprotectin axis as targeted therapy for HR-/HER2+ breast cancers. Genes Dev. *29*, 1631–1648. https://doi.org/10.1101/gad.262642.115.
32. Zambetti, N.A., Ping, Z., Chen, S., Kenswil, K.J.G., Mylona, M.A., Sanders, M.A., Hoogenboezem, R.M., Bindels, E.M.J., Adisty, M.N., Van Strien, P.M.H., et al. (2016). Mesenchymal Inflammation Drives Genotoxic Stress in Hematopoietic Stem Cells and Predicts Disease Evolution in Human Pre-leukemia. Cell Stem Cell *19*, 613–627. https://doi.org/10.1016/j.stem.2016.08.021.
33. Perego, M., Tyurin, V.A., Tyurina, Y.Y., Yellets, J., Nacarelli, T., Lin, C., Nefedova, Y., Kossenkov, A., Liu, Q., Sreedhar, S., et al. (2020). Reactivation of dormant tumor cells by modified lipids derived from stress-activated neutrophils. Sci. Transl. Med. *12*, eabb5817. https://doi.org/10.1126/scitranslmed.abb5817.
34. Fenelon, J.C., Banerjee, A., and Murphy, B.D. (2014). Embryonic diapause: development on hold. Int. J. Dev. Biol. *58*, 163–174. https://doi.org/10.1387/ijdb.140074bm.
35. Schneider, R.K., Schenone, M., Ferreira, M.V., Kramann, R., Joyce, C.E., Hartigan, C., Beier, F., Brümmendorf, T.H., Germing, U., Platzbecker, U., et al. (2016). Rps14 haploinsufficiency causes a block in erythroid differentiation mediated by S100A8 and S100A9. Nat. Med. *22*, 288–297. https://doi.org/10.1038/nm.4047.
36. Liu, X., Zhang, Y., Ni, M., Cao, H., Signer, R.A.J., Li, D., Li, M., Gu, Z., Hu, Z., Dickerson, K.E., et al. (2017). Regulation of mitochondrial biogenesis in erythropoiesis by mTORC1-mediated protein translation. Nat. Cell Biol. *19*, 626–638. https://doi.org/10.1038/ncb3527.
37. Stoneley, M., Harvey, R.F., Mulroney, T.E., Mordue, R., Jukes-Jones, R., Cain, K., Lilley, K.S., Sawarkar, R., and Willis, A.E. (2022). Unresolved stalled ribosome complexes restrict cell-cycle progression after genotoxic

stress. Mol. Cell *82*, 1557–1572.e7. https://doi.org/10.1016/j.molcel.2022.01.019.

38. Lu, Y.C., Sanada, C., Xavier-Ferrucio, J., Wang, L., Zhang, P.X., Grimes, H.L., Venkatasubramanian, M., Chetal, K., Aronow, B., Salomonis, N., and Krause, D.S. (2018). The Molecular Signature of Megakaryocyte-Erythroid Progenitors Reveals a Role for the Cell Cycle in Fate Specification. Cell Rep. *25*, 2083–2093.e4. https://doi.org/10.1016/j.celrep.2018.10.084.
39. Nemeth, E., Rivera, S., Gabayan, V., Keller, C., Taudorf, S., Pedersen, B.K., and Ganz, T. (2004). IL-6 mediates hypoferremia of inflammation by inducing the synthesis of the iron regulatory hormone hepcidin. J. Clin. Invest. *113*, 1271–1276. https://doi.org/10.1172/JCI20945.
40. Hirano, T. (2021). IL-6 in inflammation, autoimmunity and cancer. Int. Immunol. *33*, 127–148. https://doi.org/10.1093/intimm/dxaa078.
41. Chen, X., Eksioglu, E.A., Zhou, J., Zhang, L., Djeu, J., Fortenbery, N., Epling-Burnette, P., Van Bijnen, S., Dolstra, H., Cannon, J., et al. (2013). Induction of myelodysplasia by myeloid-derived suppressor cells. J. Clin. Invest. *123*, 4595–4611. https://doi.org/10.1172/JCI67580.
42. Basiorka, A.A., McGraw, K.L., Eksioglu, E.A., Chen, X., Johnson, J., Zhang, L., Zhang, Q., Irvine, B.A., Cluzeau, T., Sallman, D.A., et al. (2016). The NLRP3 inflammasome functions as a driver of the myelodysplastic syndrome phenotype. Blood *128*, 2960–2975. https://doi.org/10.1182/blood-2016-07-730556.
43. Yang, Y., Akada, H., Nath, D., Hutchison, R.E., and Mohi, G. (2016). Loss of Ezh2 cooperates with Jak2V617F in the development of myelofibrosis in a mouse model of myeloproliferative neoplasm. Blood *127*, 3410–3423. https://doi.org/10.1182/blood-2015-11-679431.
44. Leimkühler, N.B., Gleitz, H.F.E., Ronghui, L., Snoeren, I.A.M., Fuchs, S.N.R., Nagai, J.S., Banjanin, B., Lam, K.H., Vogl, T., Kuppe, C., et al. (2021). Heterogeneous bone-marrow stromal progenitors drive myelofibrosis via a druggable alarmin axis. Cell Stem Cell *28*, 637–652.e8. https://doi.org/10.1016/j.stem.2020.11.004.
45. Elliott, M.A., Verstovsek, S., Dingli, D., Schwager, S.M., Mesa, R.A., Li, C.Y., and Tefferi, A. (2007). Monocytosis is an adverse prognostic factor for survival in younger patients with primary myelofibrosis. Leuk. Res. *31*, 1503–1509. https://doi.org/10.1016/j.leukres.2006.12.025.
46. Tefferi, A., Shah, S., Mudireddy, M., Lasho, T.L., Barraco, D., Hanson, C.A., Ketterling, R.P., Elliott, M.A., Patnaik, M.S., Pardanani, A., and Gangat, N. (2018). Monocytosis is a powerful and independent predictor of inferior survival in primary myelofibrosis. Br. J. Haematol. *183*, 835–838. https://doi.org/10.1111/bjh.15061.
47. Calvo, X., Roman-Bravo, D., Garcia-Gisbert, N., Rodriguez-Sevilla, J.J., Garcia-Avila, S., Florensa, L., Gibert, J., Fernández-Rodríguez, C., Salido, M., Puiggros, A., et al. (2022). Outcomes and molecular profile of oligomonocytic CMML support its consideration as the first stage in the CMML continuum. Blood Adv. *6*, 3921–3931. https://doi.org/10.1182/bloodadvances.2022007359.
48. Weiss, G., Ganz, T., and Goodnough, L.T. (2019). Anemia of inflammation. Blood *133*, 40–50. https://doi.org/10.1182/blood-2018-06-856500.
49. Garcia, V., Perera, Y.R., and Chazin, W.J. (2022). A Structural Perspective on Calprotectin as a Ligand of Receptors Mediating Inflammation and Potential Drug Target. Biomolecules *12*, 519. https://doi.org/10.3390/biom12040519.
50. Dimitrov, D., Türei, D., Garrido-Rodriguez, M., Burmedi, P.L., Nagai, J.S., Boys, C., Ramirez Flores, R.O., Kim, H., Szalai, B., Costa, I.G., et al. (2022). Comparison of methods and resources for cell-cell communication inference from single-cell RNA-Seq data. Nat. Commun. *13*, 3224. https://doi.org/10.1038/s41467-022-30755-0.
51. Street, K., Risso, D., Fletcher, R.B., Das, D., Ngai, J., Yosef, N., Purdom, E., and Dudoit, S. (2018). Slingshot: cell lineage and pseudotime inference for single-cell transcriptomics. BMC Genom. *19*, 477. https://doi.org/10.1186/s12864-018-4772-0.
52. Love, M.I., Huber, W., and Anders, S. (2014). Moderated estimation of fold change and dispersion for RNA-seq data with DESeq2. Genome Biol. *15*, 550. https://doi.org/10.1186/s13059-014-0550-8.
53. Zhu, A., Ibrahim, J.G., and Love, M.I. (2019). Heavy-tailed prior distributions for sequence count data: removing the noise and preserving large differences. Bioinformatics *35*, 2084–2092. https://doi.org/10.1093/bioinformatics/bty895.
54. Wu, T., Hu, E., Xu, S., Chen, M., Guo, P., Dai, Z., Feng, T., Zhou, L., Tang, W., Zhan, L., et al. (2021). clusterProfiler 4.0: A universal enrichment tool for interpreting omics data. Innovation *2*, 100141. https://doi.org/10.1016/j.xinn.2021.100141.
55. Yu, G., Wang, L.G., Han, Y., and He, Q.Y. (2012). clusterProfiler: an R package for comparing biological themes among gene clusters. OMICS *16*, 284–287. https://doi.org/10.1089/omi.2011.0118.
56. Liberzon, A., Birger, C., Thorvaldsdóttir, H., Ghandi, M., Mesirov, J.P., and Tamayo, P. (2015). The Molecular Signatures Database (MSigDB) hallmark gene set collection. Cell Syst. *1*, 417–425. https://doi.org/10.1016/j.cels.2015.12.004.
57. Köhler, S., Gargano, M., Matentzoglu, N., Carmody, L.C., Lewis-Smith, D., Vasilevsky, N.A., Danis, D., Balagura, G., Baynam, G., Brower, A.M., et al. (2021). The Human Phenotype Ontology in 2021. Nucleic Acids Res. *49*, D1207–D1217. https://doi.org/10.1093/nar/gkaa1043.
58. Hao, Y., Hao, S., Andersen-Nissen, E., Mauck, W.M., 3rd, Zheng, S., Butler, A., Lee, M.J., Wilk, A.J., Darby, C., Zager, M., et al. (2021). Integrated analysis of multimodal single-cell data. Cell *184*, 3573–3587.e29. https://doi.org/10.1016/j.cell.2021.04.048.
59. Hänzelmann, S., Castelo, R., and Guinney, J. (2013). GSVA: gene set variation analysis for microarray and RNA-seq data. BMC Bioinf. *14*, 7. https://doi.org/10.1186/1471-2105-14-7.
60. Cox, J., Matic, I., Hilger, M., Nagaraj, N., Selbach, M., Olsen, J.V., and Mann, M. (2009). A practical guide to the MaxQuant computational platform for SILAC-based quantitative proteomics. Nat. Protoc. *4*, 698–705. https://doi.org/10.1038/nprot.2009.36.
61. Wiśniewski, J.R., Hein, M.Y., Cox, J., and Mann, M. (2014). A "proteomic ruler" for protein copy number and concentration estimation without spike-in standards. Mol. Cell. Proteomics *13*, 3497–3506. https://doi.org/10.1074/mcp.M113.037309.
62. Hafemeister, C., and Satija, R. (2019). Normalization and variance stabilization of single-cell RNA-seq data using regularized negative binomial regression. Genome Biol. *20*, 296. https://doi.org/10.1186/s13059-019-1874-1.

STAR★METHODS

KEY RESOURCES TABLE

REAGENT or RESOURCE	SOURCE	IDENTIFIER
Antibodies		
CD14-Pacific blue	BD-Biosciences	558121; RRID: AB_397041
CD300E-PE	Biolegend	339704; RRID:AB_2074099
CD34-APC	Sony	RT-2317550; clone 581
CD36-PECy7	Biolegend	336222; RRID: AB_2716142
CD45-BUV510	Biolegend	304036; RRID: AB_2561940
CD64-PerCp Cy5.5	Biolegend	305024; RRID: AB_2561585
HLA-DR-BV650	BD Biosciences	564231; RRID: AB_2738685
Biological samples		
Human bone marrrow $CD34^+$ cells	Lonza	2H-101B
Chemicals, peptides, and recombinant proteins		
Recombinant human IL-6	Peprotech	300-06
Recombinant human M-CSF	Peprotech	300-25
Recombinant human calprotectin	Biolegend	753406
Stem cell factor	Peprotech	300-07
FLT3 ligand	Peprotech	300-19
Thrombopoietin	Peprotech	300-18
UM729	Stemcell Technologies	72332
StemRegenin	Stemcell Technologies	72342
StemSpan SFEM II	Stemcell Technologies	09655
Recombinant human G-CSF	Preprotech	300-23
Recombinant human IL-3	Peprotech	200-03
Recombinant human EPO	Gibco	PHC254
Critical commercial assays		
Bio-Plex Pro-T Human chemokine panel 40-plex assay	Bio-Rad	171AK99MR2
Calprotectin R-plex human antibody sets	MSD	K151YBR-2
ATAC-Seq kit	Active Motif	53150
Direct-zol RNA microprep	Zymo research	R2062
TRI reagent	Zymo research	R2050-1-200
Mastermix Superscript & trade	Thermofisher	11756050
Methocult SF H4436	Stencell technologies	04436
Deposited data		
scRNAseq data: DAC Calprotectin *in vitro* effects on human early hematopoiesis	EGA public data repository :	EGAD50000000659 (DUO:0000004)
Azimuth's Human Bone Marrow	Azimuth consortium	https://azimuth.hubmapconsortium.org/
Halmark	GSEA	https://www.gsea-msigdb.org/gsea/msigdb/human/collections.jsp
HPO - Human Phenotype Ontology	The Jackson Laboratory	https://hpo.jax.org/
KEGG	Genome Japan	https://www.genome.jp/kegg/pathway.html
MSidDBr package v7.5.1	GSEA	https://www.gsea-msigdb.org/gsea/msigdb
UniProt-Swiss-Prot	Uniprot	https://www.uniprot.org/
COVID dataset	Cheong et al.[26]	GSE196990
MPN dataset	Psaila et al.[25]	GSE144568
CMML dataset	Ferrall-Fairbanks et al.[27]	GSE211033

(*Continued on next page*)

Continued

REAGENT or RESOURCE	SOURCE	IDENTIFIER
AML dataset	Bottomly et al.[29]	https://cbioportal.org/
scRNAseq data set	EGA	EGAD50000000659 (Data Use Ontology DUO:0000004) "DAC Calprotectin *in vitro* effects on human early hematopoiesis"
Proteomic data set	Pride (ProteomeXchange)	ProteomeXchange accession: PXD057999; Project Webpage: http://www.ebi.ac.uk/pride/archive/projects/PXD057999 FTP Download: https://ftp.pride.ebi.ac.uk/pride/data/archive/2024/11/PXD057999
GO	Gene Ontology	https://geneontology.org/
Oligonucleotides		
S100A8 Forward	Eurogentec	*5'-CAACACTGATGGTGCAGTTAACTTC-3'*
S100A8 Reverse	Eurogentec	*5'-CTGCCACGCCCATCTTTATC-3'*
S100A9 Forward	Eurogentec	*5'-CTGAGCTTCGAGGAGTTCATCA-3'*
S100A9 Reverse	Eurogentec	*5'-CGTCACCCTCGTGCATCTTC-3'*
GUS Forward	Eurogentec	*5'-GAAAATATGTGGTTGGAGAGCTCATT-3'*
GUS Reverse	Eurogentec	*5'-CCGAGTGAAGATCCCCTTTTTA-3'*
RPL32 Forward	Eurogentec	*5'-TGTCCTGAATGTGGTCACCTGA-3'*
RPL32 Reverse	Eurogentec	*5'-CTGCAGTCTCCTTGCACACCT-3'*
PPIA Forward	Eurogentec	*5'-GTCGACGGCGAGCCC-3'*
PPIA Reverse	Eurogentec	*5'-TCTTTGGGACCTTGTCTGCAA-3'*
Software and algorithms		
Annotation Dbi package		https://bioconductor.org/packages/release/bioc/html/AnnotationDbi.html
Bowtie2	v2.0.14	https://bowtie-bio.sourceforge.net/bowtie2/index.shtml
Clusterprofiler package	v4.6	https://bioconductor.org/packages/release/bioc/html/clusterProfiler.html
DESeq2	v1.38.3	https://bioconductor.org/packages/release/bioc/html/DESeq2.html
Factoextra package	v1.0.7	https://cran.r-project.org/web/packages/factoextra/index.html
Fast integration using reciprocal PCA	V4.3	https://satijalab.org/seurat/archive/v4.3/integration_large_datasets
Findmakers in Seurat	v.4	https://satijalab.org/seurat/reference/findmarkers https://
GENCODE	v24lift37	www.gencodegenes.org/
Harmony package	v 0.1.0	https://cran.r-project.org/web/packages/harmony/index.html
HTSeq	0.5.4p5	https://htseq.readthedocs.io/en/latest/
Manager Software	v6.1	https://www.bio-rad.com/
MaxQuant	V1.5.2.8	https://www.maxquant.org/
MSD Discovery workbench	v4.0	https://software.mesoscale.com/
MSidDBr package	v7.5.1	https://www.gsea-msigdb.org/gsea/msigdb
Perseus	V1.5.1.6	https://maxquant.net/perseus/
R	V4.2.2	https://www.npackd.org/p/r/4.2.2/
SCTransform	V2	https://satijalab.org/seurat/archive/v4.3/sctransform_v2_vignette https://bioconductor.org
Slingshot	v2.6	https://www.npackd.org/p/r/4.2.2/
TopHat2	v2.1.0	https://ccb.jhu.edu/software/tophat/index.shtml

EXPERIMENTAL MODEL AND STUDY PARTICIPANT DETAILS

This study was entirely performed on human primary cells in *ex vivo* culture. Human $CD34^+$ progenitors were collected from the bone marrow of healthy adult donors (N=10, Lonza, 2M-101B) or from cord blood donors (N=6, Cell Therapy Unit, Saint-Louis Hospital, Paris) or from the peripheral blood of patients with JAK2-V617F $JAK2^{V617F}$ MF (N=3) with written informed consent. Patient sample collection was performed in accordance with the Declaration of Helsinki following study approval by the Ethics Committee Ile de France III (Institutional review board IDRCB 2015-A01048-41- Protocol C14/42). All the cell samples proposed by Lonza were from male donors. $JAK2^{V617F}$ MF cells were collected from male patients as well.

METHOD DETAILS

Cell cultures

$CD34^+$ cells initially sorted by AutoMacs system (Miltenyi Biotech) and frozen in FBS-DMSO 10% were thawed, and cultured at 0.15×10^6 cells/mL, either in MEM-alpha medium (Gibco) supplemented with 10% fetal calf serum (FCS, Eurobioscientific) and 2 mM L-glutamine (all from Gibco) or in StemSpan™ SFEM II (StemCell Technologies). Media were supplemented with 1% penicillin/streptomycin (P/S) and recombinant human FMS-related tyrosine kinase 3 ligand (FLT3L), Stem Cell Factor (SCF) and thrombopoietin (TPO), all at 40 ng/mL (PeproTech) at 37°C, 5% CO2, and 20% O2. UM729 (35 nM) and StemRegenin 1 (75 nM) (both from StemCell Technologies) were added to StemSpan™. After 48 hours, the cells were plated in fresh medium in the absence or presence of 100 ng/mL recombinant human IL6 (PeproTech), CAL (10 000 ng/mL, BioLegend), or their combination (IL6_CAL). The cells were collected at 24 or 48 hours for bulk RNA sequencing or were diluted on day 4 with fresh cytokines and treatments to be harvested using PBS/EDTA 0.1% (Prolabo) on day 7, together with their supernatant.

We also performed independent erythroid cell cultures from human $CD34^+$ progenitors of adult healthy donor bone marrows as described.[19] After 48 hours in StemSpan™ SFEM II medium with SCF, UM729 and StemRegenin 1, cells were plated at 0.8×10^6 cells/mL in Iscove's modified Dulbecco medium (IMDM; Life Technologies, Grand Island, NY) supplemented with 15% serum substitute (StemCell Technologies, Vancouver, Canada), 40 ng/mL FLT3L, 100ng/mL SCF, 1 UI/mL IL3, 2 UI/mL erythropoietin (EPO, Roche Diagnosis, Basel, Switzerland), 1 μM dexamethasone (DEXA, Sigma-Aldrich, Saint-Louis, MI) for 5 days. From day 6, the cells were maintained with SCF, EPO and DEXA for 2 days, then with SCF and EPO for 2 days and from d10 with EPO alone. When indicated, IL6 (10 ng/mL) and CAL (10 000ng/mL) were added at day 0 and renewed every 3 days. Erythroid differentiation was assessed by the cytological examination of May-Grünwald-Giemsa-stained cytospins. Cells were harvested at day 5 and seeded at 4×10^3 cells/mL with or without CAL in methylcellulose for colony-forming cell assays in the presence of EPO, SCF, IL3, IL6, G-CSF, and GM-CSF (MethoCult™ SF H4436, StemCell Technologies, Vancouver, Canada). Colonies of burst-forming unit-erythroid (BFU-E) and colony-forming unit (CFU)-granulomonocytic (GM), granulocytic (G) or monocytic (M) types were enumerated after 14 days of the methylcellulose culture. Cells were also collected at day 7, day 12 and day 15 for proteomic analyses.

Cord blood $CD34^+$ cells (7.5×10^4 /ml) were cultured in SFEM II in the presence of 40 ng/mL SCF and 10 ng/mL M-CSF for 7 days, with or without IL6 or CAL, before cell count and flow cytometry analysis of cell surface markers at the surface of CD34-negative cells, especially CD64 and CD300E, and RT-qPRC analysis of *S100A8* and *S100A9* gene expression, using *GUS*, *PPIA* and *RPL32* as housekeeping genes (Primers in the key resources table).

Bulk RNA-seq

Total RNA was collected from cells cultured for 24 or 48 hours using TRI Reagent and Direct-zol™ RNA Microprep (both from Zymo Research). RNA integrity (score $\geq$ 7.0) was checked on a fragment analyzer (Agilent) and quantified using a Qubit (Invitrogen). A SureSelect Automated Strand Specific RNA Library Preparation Kit was used according to the manufacturer's instructions with the Bravo Platform. Briefly, 100 ng of total RNA was used for poly(A) mRNA selection using oligo(dT) beads and subjected to thermal mRNA fragmentation before conversion into double-stranded DNA for library preparation. The final libraries were barcoded, purified, pooled and subjected to paired-end sequencing on a NovaSeq-6000 sequencer (Illumina).

Single-cell RNA sequencing

Single-cell suspensions (to reach ~10,000 individual cells per sample) were loaded onto a Chromium Single Cell Chip (10x Genomics) according to the manufacturer's instructions for coencapsulation with a barcoded gel using a Chromium Controller (10X Genomics). Captured mRNAs were barcoded during cDNA synthesis using the Chromium Next GEM Single Cell 3' GEM, Library & Gel Bead Kit v3.1 (10X Genomics) according to the manufacturer's instructions. All samples were prepared at the same time per donor under the 4 conditions and processed simultaneously with a Chromium Controller (10X Genomics), and the resulting libraries were prepared in a single batch. All the libraries were pooled for sequencing with an 8-base index read, a 28-base Read1 containing a cell identifying barcode with unique molecular identifiers (UMIs), and a 91-base Read2 containing transcript sequences on a NovaSeq 6000 (Illumina).

Assays for transposase-accessible chromatin using sequencing

The assay for transposase-accessible chromatin with sequencing (ATAC-seq) was performed on 100,000 cells generated from HD and MF CD34^{+} progenitors after 7 days in liquid culture in the absence or presence of IL6 using an ATAC-Seq kit (Active Motif). After centrifugation, the supernatant was discarded, and the cells were collected in 100 μl of ice-cold ATAC lysis buffer. After centrifugation, the supernatant was discarded, and the nuclei were subjected to a tagmentation reaction (30 min at 37°C) and DNA purification according to the manufacturer's instructions. The purified tagged DNA was amplified 10-fold by PCR with a combination of the indexed primers i7 and i5 followed by SPRI clean-up before quality control using a fragment analyzer (Agilent). The final libraries were pooled together in equal concentrations and subjected to paired-end sequencing (100 cycles, 2x50) using a NovaSeq-6000 sequencer (Illumina).

Cytokine level measurements

Culture supernatants were collected after sample centrifugation at 1500 rpm for 5 min and stored at -80°C. Medium without cells was used as a control. Aliquots were centrifuged at 1500 rpm for 15 min at 4°C, diluted 1:4 and analyzed using a Bio-Plex ProTM Human Chemokine Panel 40-plex Assay (Bio-Rad). Acquisitions and analyses were performed on a Bio-Plex 200 system with Manager 6.1 Software (Bio-Rad). Soluble CAL was measured using R-plex Human Antibody Sets (Meso Scale Discovery), a MESO QuickPlex SQ120 reader and MSD Discovery Workbench 4.0.

Quantitative proteomics and data analysis

The cells were collected on days 7, 12 and 15 of EPO-driven liquid culture. Label-free quantification (LFQ) proteomic experiments were performed as described previously.[20] Mass spectrometry (MS) data were processed with MaxQuant version 1.5.2.8 using human sequences from the UniProt-Swiss-Prot database (UniProt, release 2015-02) with a false discovery rate (FDR) below 1% for both peptides and proteins.[51]

QUANTIFICATION AND STATISTICAL ANALYSIS

Statistical analysis

Statistical tests are indicated in the figure legends. The p-values of the tests are expressed as follows: * $p<0.05$, ** $p<0.01$, *** $p<0.001$, **** $p<0.0001$. In the absence of precision, the test is not significant.

Bulk RNA-seq

The raw reads were mapped to the hg19 genome with TopHat2 (v2.0.14)/Bowtie2 (v2.1.0). The number of reads per gene (GENECODE gene annotation v24lift37) was counted using HTSeq (0.5.4p5). Differential expression analysis was performed with DESeq2 v1.38.3 (50),[50] accounting for the donor effect in the mode, after filtering out genes that did not have at least 10 counts in at least 1 sample. MA plots were drawn using the shrunk Log2FoldChange from DESeq2 analysis via the apeglm shrinkage method.[52] Gene set enrichment analysis (GSEA) and overrepresentation analysis (ORA) were performed with the clusterProfiler package v4.6.[53,54] Gene sets from the Hallmark, KEGG, GO, and HPO databases were retrieved from the Molecular Signatures Database (MSigDB) using the msigdbr package (v 7.5.1).[55,56] Genes we56re annotated using the mapIds function of the AnnotationDbi package. The mapped gene names were ranked according to their ''stat'' score from the differential expression analysis, and GSEA was run with a p value cutoff of 0.05, which was limited to gene sets of a size between 20 and 800 genes. The results were sorted by the NES, and the top pathways were plotted with ggplot2. Deconvolution was performed using gene set variation analysis (GSVA)[57] with the GSVA package v1.42. Homemade gene sets of hematopoietic cells based on Azimuth Human Bone Marrow reference annotation markers with a few additional known genes (Table S1) were used to measure enrichment scores (GSVA method, with kcdf set to Poisson).

Single-cell RNA sequencing

The raw BCL files were demultiplexed using bcl2fastq (version 2.20.0.422 from Illumina), and read quality control was performed using fastqc (version 0.11.9). Reads were pseudomapped to the Ensembl reference transcriptome v99 (*Homo sapiens* GRCh38 built with Kallisto, version 0.46.2). The index was prepared with the kb-python (version 0.24.4) wrapper of Kallisto. Barcode correction was performed using the whitelist provided by the manufacturer, and gene-based read quantification was performed with BUStools (version 0.40.0). Empty droplets were detected using the emptyDrops function from the dropletUtils package (version 1.10.3), and barcodes with a p value < 0.001 (Benjamini–Hochberg-corrected) were considered for analysis. The count matrix was filtered to exclude genes detected in fewer than five cells, cells with fewer than 1500 UMIs or fewer than 200 detected genes, and cells with a proportion of mitochondrial transcripts greater than 20%. Cell cycle scoring was performed using the CellcycleScoring function of the Seurat package (version 4.0.4) and the cyclone function of Scran (version 1.20.1). Doublets were discarded using scDblFinder (version 1.6.0) and scds (version 1.8.0). We manually verified that cells identified as doublets did not correspond to cells in the G2/M phase. Datasets were integrated using the Harmony method and merged using Seurat (version 4.0.4; 56), and the SCTransform normalization method[58] was used to normalize and scale the data, select 3000 highly variable genes and regress out bias factors. The reduced PCA spaces were used as input for the HarmonyMatrix function implemented in the Harmony package (version

0.1.0), where the batch effect (donor: D16, D19, D22, D23, DAR, PRU, VAR) was regressed. The shared space output by Harmony was used for clustering. The optimal number of dimensions was evaluated by assessing a range of reduced Harmony spaces using 3 to 49 dimensions, with a step of 2. For space, Louvain clustering of cells was performed using a range of values for the resolution parameter from 0.1 to 1.2 with a step of 0.1. The optimal space was the combination of kept dimensions and clustering resolution resolving the best structure (cluster homogeneity and compacity) in UMAP (19 PCs, resolution 0.1 and 0.6) (52). Marker genes for Louvain clusters were identified through a ''one versus others'' differential expression analysis using the Wilcoxon test through the FindAllMarkers function from Seurat, considering only genes with a minimum log fold change of 0.5 in at least 50% of cells from one of the groups compared and FDR-adjusted p values <0.05 (Benjaminin–Hochberg method) and annotated using the celltype.l2 annotation markers of Azimuth's Human Bone Marrow dataset, to which a few known genes were added to generated signatures (Table S1) that were scored using AddModuleScore and visualized by UMAP using FeaturePlot. Differential gene expression analysis was performed using FindMarkers in Seurat v.4 (logfc threshold, 0.25; p value, 0.05; test.use set to "wilcox"), and the results were plotted with the EnhancedVolcano function and used for overrepresentation analysis (ORA) with the clusterProfiler package v4.6.[53,54] Gene sets from the Hallmark, KEGG, GO, and HPO databases were retrieved from the Molecular Signatures Database (MSigDB) using the msigdbr package (v 7.5.1).[55,56] The q value cutoff was set to 0.05, with the other parameters set to the default values. ORA pathways were sorted by their adjusted p value, and those with the highest padj were selected for plotting. When plots combined several conditions or clusters, the top pathways were combined. Pseudobulk analysis was performed on the normalized counts. The mean expression of every gene was calculated with the AverageExpression function of Seurat by clustering (every cluster had 28 pseudobulk values for each gene) before principal component analysis (PCA) using the factoextra package v1.0.7. Trajectory analysis was performed using slingshot v2.6.,[59] using cluster 9 at a resolution of 0.6 as the starting cluster (lowest pseudotime with high HSC signature). Given the size of our dataset, we set the approx_points argument to 100, as suggested in the slingshot vignette (https://bioconductor.org/packages/devel/bioc/vignettes/slingshot/inst/doc/vignette.html). The pseudotime of cells in each identified lineage was retrieved and plotted by UMAP.

Cytokine level measurements

Each sample was assayed twice, and the average value was taken as the final result. Differential expression analysis was performed on R (v4.2.2), measuring the log2-fold change in the mean concentration of each cytokine in each condition and measuring the p value of the concentration of each cytokine in each condition using a paired Wilcoxon test to account for donors. The adjusted p value was calculated using Benjamini and Hochberg corrections. IL6 quantification was excluded under the IL6 and IL6_CAL treatments, while CAL quantification was excluded under the CAL and IL6_CAL treatments.

Quantitative proteomics and data analysis

LFQ results from MaxQuant were imported into Perseus software (version 1.5.1.6). We calculated average values of duplicates and calculated the protein copy number per cell by using the Protein Ruler plugin of Perseus by standardizing the total histone MS signal.[60,61] Focusing on the dynamics of ribosomal proteins, we subtracted the mean concentration of each protein on day 12 from its mean concentration on day 15 of EPO-driven liquid culture.

CAL signature validation

The gene expression signature of the MEP2 cluster was used to score MEP2-like cells in other datasets using Seurat's AddModuleScore function. Cells with a score > 0.1 for the MEP2-like signature were used to test the CAL_up and CAL_down signatures obtained by combining analyses of HD and MF samples; i.e., these signatures included genes up- and downregulated under CAL conditions in both HD and MF samples. CAL_up and CAL_down signatures were scored using the Seurat function AddModuleScore in other datasets. Each individual sample of a COVID-19 dataset (GEO: GSE196990)[26] was normalized, and the variance was stabilized with SCTransform (with vst.flavor set to 'v2', i.e., using the glmGamPoi function) before merging.[62] PCA was performed with default parameters, and 30 PCs were used for UMAP embedding and clustering. The cluster resolution was set at 0.1. Data from the MPN dataset (GEO: GSE144568)[25] were processed following the Seurat vignette ''Fast integration using reciprocal PCA (RPCA)'' v4.3, and PCA was performed with default parameters. Integration was performed with the Harmony package to regress donor effects using sampleID metadata. Thirty PCs were used for UMAP embedding and clustering. The CMML dataset (GEO: GSE211033)[27] was normalized, and the variance was stabilized with SCTransform before fast integration using reciprocal PCA. Patients with CMML and monocytosis of at least 1 G/L were analyzed. The AML bulk bone marrow cell RNAseq dataset (https://www.cbioportal.org/study/summary?id=aml_ohsu_2022)[29] was separated according to the WBC fraction of monocytes annotated for 271 out of 362 samples before exploring the CAL_up and CAL_down signatures using the GSVA method.